Geogrid stabilisation in asphalt paved roads

Quantification of the modulus improvement factor

S. T. van der Zee

Middelburg, August 5th, 2019

UNIVERSITY OF APPLIED SCIENCES

Tensar®

Geogrid Stabilisation in asphalt paved roads

Quantification of the modulus improvement factor

Author:	S. T. van der Zee
Student Number:	00071210
Study year:	2018-2019
Semester:	8th
Report type:	Graduation thesis
Course:	Civil Engineering
Educational Institute:	HZ University of Applied Sciences
Supervisor:	Mr. Ir. P. Dekker
Company:	Tensar International
Company supervisor:	Mr. L. Kuljanski

Place of publication:	Middelburg
Date:	August 5th, 2019
Version:	C

Preface

Are you familiar with geogrids? As a civil engineering student, I was not. Until a presentation by Tensar about the many applications of geogrids caught my attention. I decided at the time that I wanted to learn more about this.

Since the introduction of geogrids in Dutch road construction in the 1980s, their use has been subjected to developments. New research leads to new insights and new insights are processed in new calculation methods. This research contributes to this development of new insights and new calculation methods.

Based on practical experience, Tensar concluded that the current calculation method for stabilizing geogrids, had room for improvement. Therefore, they asked me the following question: "How can we develop a new mechanistic-empirical method, to calculate the effect of geogrid stabilisation on the foundation of asphalt paved roads?" This method had to be based on the 'modulus improvement factor' and use rut formation data from 'heavy vehicle simulator' research.

For a period of six months, I immersed myself in geotechnics and road design to find an answer to this question. I have been assisted by my graduation supervisor, dhr. L. Kuljanski, and my supervisor from the HZ University of Applied Sciences, dhr. P. Dekker. I have learned a lot from them, and they were always ready to answer my questions

I would like to thank my supervisors for the good cooperation, as well as my other colleagues at Tensar. I also want to thank my friends, family and in particular my parents. They helped me get things back on track, when I was struggling.

I hope that my research will give you a better understanding of how geogrids work.

Siebe Theodoor van der Zee

Middelburg, August 5th, 2019

Voorwoord

Bent u bekend met geogrids? Als student civiele techniek was ik dat niet namelijk, totdat een presentatie van Tensar over de vele toepassingen van geogrids mijn aandacht greep. Het was dat moment dat ik besloot meer over geogrids te willen weten.

Sinds de introductie van geogrids in de Nederlandse wegenbouw sector in de jaren tachtig, is het gebruik daarvan onderhevig aan ontwikkeling. Nieuw onderzoek leidt tot nieuwe inzichten en nieuwe inzichten worden verwerkt in nieuwe rekenmethoden. Dit onderzoek draagt daar ook een deel aan bij.

Op basis van praktijkervaringen concludeerde Tensar dat de huidige rekenmethode voor stabiliserende geogrids enkele tekortkomingen kent. Ze stelde mij daarom de volgende vraag: “Hoe kunnen we een nieuwe mechanistisch-empirische methode ontwikkelen, om het effect van geogrid stabilisatie op de fundering van asfalt verharde wegen, te berekenen?” Deze methode moest gebaseerd zijn op de ‘modulus improvement factor’ en spoorvorming informatie gebruiken van ‘heavy vehicle simulator’ onderzoek.

Gedurende een periode van zes maanden, heb ik mij ondergedompeld in de geotechniek en wegenbouw, om deze vraag te kunnen beantwoorden. Ik werd hierin bijgestaan door mijn afstudeerbegeleider, Leo Kuljanski, en mijn begeleider vanuit mijn opleiding, Piet Dekker. Ik heb veel van hen mogen leren en zij stonden altijd klaar om mijn vragen te beantwoorden.

Ik wil mijn begeleiders graag bedanken voor de goede samenwerking, evenals mijn andere collega's bij Tensar. Ook gaat mijn dank uit naar mijn vrienden, familie en in het bijzonder mijn ouders. Zij hielpen mij de draad weer op te pakken, wanneer het tegen zat.

Ik hoop dat mijn onderzoek u een beter inzicht geeft in de werking van geogrids.

Siebe Theodoor van der Zee

Middelburg, August 5th, 2019

Abstract

The use of TriAx geogrids to stabilise the granular base layer of asphalt paved roads, is ever increasing. However, the effect a stabilising geogrid has on the entire pavement structure is still derived from a foundation reduction factor, instead of being calculated directly. Practical experience showed that this can lead to inaccurate or conservative designs.

The goal of this study is to create a new mechanistic-empirical calculation method, based on the modulus improvement factor of geogrid stabilised granular base layers in asphalt paved roads. Additionally, this calculation method must be able to determine the influence of the type of geogrid, the foundation thickness and the subgrade stiffness. Hereto the following research question has been posed: "*What is the Modulus Improvement Factor of a by TriAx geogrids stabilised granular base layer for Mechanistic-Empirically designed asphalt pavements, in relation to the geogrid type, foundation thickness and subgrade stiffness?"*

The calculation method created to answer this question, combines linear elastic calculation software with asphalt strain functions. For calibration, it uses rut formation data acquired from full-scale Heavy Vehicle Simulator tests. The method was applied in a practical case to design several pavement structure variants. A life cycle cost analysis and CO2 emissions estimate were made to compare the variants.

To conclude this study, a detailed recommendation was made for further research, to increase the validity of this study's findings.

Samenvatting

Er wordt in toenemende mate gebruik gemaakt van TriAx geogrids om de fundering van wegen met asfaltverhardingen te stabiliseren. Het effect van een stabiliserend geogrid op de gehele verhardingsconstructie wordt echter nog vaak afgeleid van een fundering reductiefactor, in plaats van dat het direct wordt berekend. Uit praktijkervaring blijkt dat dit kan leiden tot onnauwkeurige of conservatieve ontwerpen.

Het doel van deze studie is het creëren van een nieuwe mechanistisch-empirische rekenmethode, gebaseerd op de 'Modulus Improvement factor' van met geogrids gestabiliseerde funderingen in verharde wegen. Deze rekenmethode moet verder in staat zijn de invloed van het type geogrid, de funderingsdikte en de stijfheid van de ondergrond, te bepalen. De hiertoe opgestelde onderzoeksvraag luidt: "*Wat is de 'Modulus Improvement Factor' van een met TriAx geogrids gestabiliseerde fundering voor mechanisch-empirisch ontworpen asfaltverhardingen, in relatie tot het type geogrid, de funderingsdikte en de stijfheid van de ondergrond?"*

De rekenmethode die is gecreëerd om deze vraag te beantwoorden, combineert lineaire elastische berekeningssoftware met asfalt vermoeiingslijnen. Ter kalibratie gebruikt de rekenmethode spoorvorming informatie, verkregen uit 'Heavy Vehicle Simulator' onderzoek van verharde wegen op ware schaal. De rekenmethode werd in een bestaand project toegepast om verschillende wegontwerpen te maken. Een levenscycluskostenanalyse en een schatting van de CO2-uitstoot zijn gemaakt om de varianten te vergelijken.

Ter afsluiting van deze studie, werd een gedetailleerde aanbeveling gedaan voor verder onderzoek, om de validiteit van de bevindingen van deze studie te verhogen.

Table of Contents

List of figures

List of tables

List of abbreviations

APT:	Accelerated Pavement Testing
AASHTO:	American Association of State Highway and Transportation Officials
CBR:	California Bearing Ratio
CROW:	Non-profit foundation (name)
CUR:	SBRCURnet (company name)
EOTA:	European Organisation for Technical Assessment
ESAL:	Equivalent Standard Axle Load
FRF:	Foundation Reduction Factor
HVS:	Heavy Vehicle Simulator
LCCA:	Life Cycle Cost Analysis
M-E:	Mechanistic-Empirical (Pavement Design Method)
MIF:	Modulus Improvement Factor
MSL:	Mechanically Stabilised Layer
NPV:	Net Present Value
OIA:	Ontwerpinstrumentarium Asfaltverhardingen
SAMDM:	South African Mechanistic Design Method
SF:	Shift Factors
SIF:	Support Improvement Factor
SN:	Structural Number
TBR:	Traffic Benefit Ratio
USACE:	United States Army Corps of Engineers

1. Introduction

Roads are an important part of a country's infrastructure. A great example of a society that has perfected the construction of roads are, the Romans. Their roads connected the corners of Europe and were of such high quality, that some even stood the test of time and remain today. The fundamentals of building a paved road were laid by the Romans, but the materials and construction methods used, developed and changed over time. From the use of stone and sand, to paving with asphalt and finally reinforcing a foundation with geosynthetic materials.

The following paragraphs start with a brief overview of road (foundation) construction throughout history, followed by the different types and functions of geogrids and the role Tensar played in this field and end with a quick look at the development of Dutch standards for building with geogrids.

1.1. Background

1.1.1. History of road foundation

Over 5000 years ago, the Egyptians build paved roads to aid in constructing the pyramids and can be marked as the beginning of the history the paved road. Early examples of paved roads that date back to around the same time were found in the Indus Valley and Mesopotamia (Lay, 1993). The first network of paved roads that connected Europe was the Roman road network, which dates back to 300 BC. These roads were meticulously planned, constructed and maintained for more than 800 years, until the fall of the Roman empire ushered in an age of neglect during which the condition of the roads deteriorated to a point where traveling was nearly impossible. It wasn't until the Napoleonic era when road construction experienced a major revival. The direction of travel was put into legislation. Civil engineers were trained, and the foundation of paved roads was standardised with the introduction of the 'steenslagweg' that had a natural stone 'paklaag' or rubble 'puinfundering' foundation consisting of multiple layers with varying particle sizes. The road foundations used in the early twentieth century do not appear to deviate significantly from those used in Roman roads almost 2000 years ago (van Gurp, van Vilsteren, van der Wegen & Hofstra, 2014).

Until the end of the second world war, the use of paving stones as a surface layer was preferred over cementitious concrete and asphalt. The fifties and sixties are characterised by asphalt pavements with sand-cement stabilised foundations. During the seventies the disadvantages of high cement content foundations showed, e.g. cracking, and the switch was made back to unbound granular aggregate foundation layers. The introduction of the equivalence factor made it possible to optimise road design by exchanging asphalt thickness for foundation thickness and vice versa. In the early eighties the need for saving on construction materials grew, which led to a serious increase of fundamental research into the use of 'new' foundation materials like geosynthetics and to define the parameters by which these new materials could be implemented and calculated with. In the following years, recycling of materials for use in road foundations became more prominent, and the requirements for pavement and foundation materials changed.

This trend of recycling, in combination with these changing requirements, led to the introduction of geosynthetics. Geosynthetics can help save on construction materials or make building on weak subgrade easier.

1.1.2. Geogrids and Tensar

Geogrids are part of the geosynthetic product group that also contains geotextiles, geomembranes and several other product types. Geogrids and geotextiles are the most commonly used geosynthetic products in pavement systems and can fulfil several different functions. Zornberg (2019) summarised all the different geosynthetic applications into six functions, as shown in Figure 2 below (barrier, filtration, drainage, separation, reinforcement and stabilization). Zornberg provides a comprehensive explanation of the functionality and objective for using geogrids and geotextiles in roadway construction, i.e. he demonstrates their versatility in use. Similar functions apply when geogrids and textiles are used in other construction fields like road construction, crane platforms, earth retaining structures or slope stabilisation.

The CROW divides geogrids with stabilising and reinforcing functions into four groups, based on their production method (see Figure 1). They then attribute different performance characteristics to each group. This will be explained further in the next chapter.

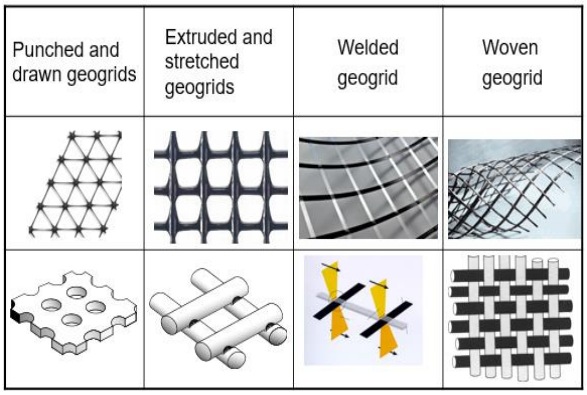

Figure 1: different types of geogrids (Kuljanksi, 2016)

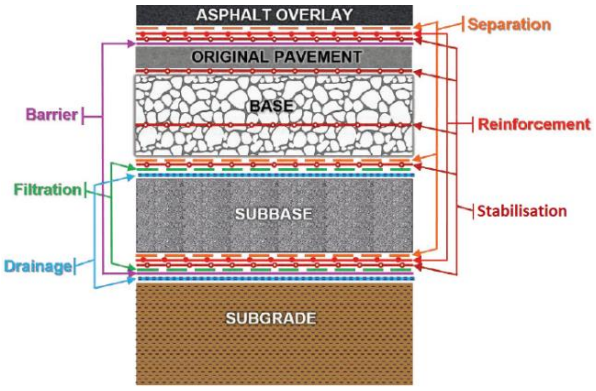

Figure 2: functions and applications of geosynthetics in roadways (Zornberg, 2019)

Tensar introduced uni-axial and biaxial geogrids in 1978. Uni-axial geogrid for reinforced earth structures and Bi-axial geogrids for road construction (Tensar, 2012). Since then, they have continually improved upon their product and calculation method. Tensar also carried out several full-scale heavy vehicle simulation tests to analyse how their geogrids function and perform. In 2008, this led to the introduction of a new type of geogrid called TriAx. The TriAx system has ribs in three directions, forming a triangle, and is better able to distribute the load acting on the soil (Dong, Han & Bai, 2011; Yang, 2012). Tensar also worked hard on defining the unique stabilizing function of their geogrids (instead of a reinforcing function), which was done by the EOTA in 2007 (EOTA, 2016). Both the BiAx and TriAx geogrids fall under the category of punched and drawn geogrids as shown in Figure 1. The cover page shows a TriAx geogrid which is used to stabilise the base layer of a road. Tensar has a large incentive, both financially

and socially, to improve the accuracy of their calculations so that they can maintain a high level of saving for both road authorities and contractors alike. By maintaining a position as market leader in geogrid stabilised pavements Tensar can continue to improve and develop her products, systems and service, with the goal of providing more benefit to her customers. There is a large social benefit to be gained for every pavement that is constructed cheaper and/or lasts longer. Cheaper and longer lasting pavements result in lower infrastructure costs, which in turn results in a lower tax burden to maintain the pavement.

1.1.3. The history of Dutch calculation methods with geogrids

The first Dutch standard that described the use of geogrids in road foundations was CUR publication 175, published in 1995. In this guideline two theoretical design methods with geogrids were introduced: the method Sellmeijer for the tension membrane effect and the Houlsby method for the lateral-restrain effect However, full scale test results with several different types of geogrids showed that both methods in CUR 175 could not predict the results of geogrid stabilisation or reinforcement.

CROW publication 157 was released seven years later and provided an operable analytical design procedure for applying geogrids in unpaved roads. In this publication the Foundation Reduction Factor (FRF) was introduced. The FRF is the factor by which the thickness of a foundation may be reduced. Foundation thickness may be reduced because of the beneficiary effect of the geogrid. The FRF is calculated depending on the type of subgrade and the type geogrid (Vega, Kwast & van Gurp, 2017).

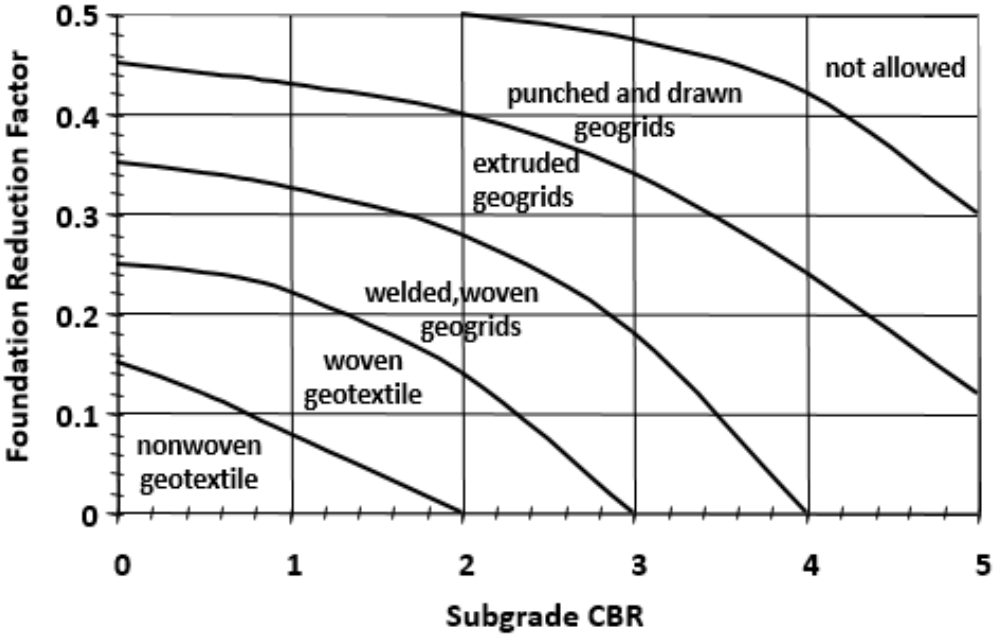

Figure 3: relation between subgrade soil stiffness and the maximum allowable foundation reduction factor, per geosynthetic product type (Vega, Kwast & van Gurp, 2017)

The design method from CROW publication 157 divided geogrids into several groups, based on their production method. The disadvantage of this method is that it offers no tools to quantify the performance of specific stabilisation or reinforcement geogrids. In this model, the enhancing effects (reinforcement and stabilisation) are dictated by the production method of the geogrid. Not on the performance characteristics of each geogrid individually. In addition, the CROW method offers no tools for applying new products and does not reflect the latest results of research and production development.

Since the release of CROW publication 157 a lot of new products had entered the market. Manufacturers wanted to use these new products in their design calculations. However, it was not possible to include new products in the existing CROW-groups (Vega, Kwast & van Gurp, 2017). Therefore, manufacturers were unable to calculate the effects of the new products.

In response to the above mentioned limitations and disadvantages, the road construction sector expressed the wish to develop a new integral document that combined (international) knowledge and experience concerning the application of geogrids as foundation stabilisation. In 2017, CUR publication 175 was revised to meet those wishes. The revised publication introduced a new user-friendly design approach for the inclusion of geogrids in unpaved roads (Vega, kwast & van Gurp, 2017).

1.2. Problem statement

The revision of CUR 175 should be regarded as an improvement. However, more improvements could be made. Based upon knowledge and expertise, Tensar believes that there are two shortcomings in the new method. First, the revised CUR 175 is only applicable to geogrid stabilisation of unpaved roads (Vega, Kwast & van Gurp, 2017). Meaning that the results of geogrid stabilisation of paved roads us sub-optimal. Which in its turn means that there is room for improvement. Secondly, the FRF stated in the revised CUR 175 is prone to inaccuracy. In order to substantiate this claim, it is necessary to understand the calculation of the FRF. The revised CUR publication 175 calculates the FRF with the following formula (Vega, Kwast & van Gurp, 2017):

$$f_{h2w} = \frac{h_{2wo}}{h_{2Go}} \cdot \frac{h_{2ww}}{h_{2Gw}}$$

Where (the Giroud-Han and Giroud-Noiray models are included in appendix B):

f_{h2w} = Reduction factor for application in Giroud-Noiray Model or Giroud-Han Model due to the influence of foundation reinforcement or stabilisation [-]

h_{2wo} = Actual layer thickness of non-reinforced test section [m]

h_{2Go} = Calculated thickness with Giroud-Noiray-model or Giroud-Han-model for the non-reinforced test section [m]

h_{2ww} = Actual layer thickness of reinforced test section [m]

h_{2Gw} = Calculated thickness with Giroud-Noiray-model or Giroud-Han-model for the reinforced test section [m]

The disadvantage of this method becomes visible when there is a large difference between the calculated and the measured (actual) thickness of the pavement structure. A large difference results in a larger FRF. A larger FRF means that the foundation thickness can be reduced more. This is beneficial for contractors because it is directly connected to lower construction costs. However, this thinner foundation is likely to be unstable and will deteriorate sooner. This means that the delivered roads are of lower quality. In the long run, this will harm both contractor and client. For the client will receive a product which is of too low a quality. In turn the contractor will be harmed in its reputation. This shows the need for a more accurate calculation method to quantify the effects of foundation reinforcement or stabilisation.

Both disadvantages (not suited for paved roads and the inaccuracy of the FRF) can be overcome by creating a mechanistic-empirical (M-E) calculation model that circumvents the FRF and is suited for calculating geogrid stabilisation on paved roads. This can be done by building the calculation model on the modulus improvement factor (MIF).

The research question is as follows: "*What is the Modulus Improvement Factor of a by TriAx geogrids stabilised granular layer for Mechanistic-Empirically designed asphalt pavements, in relation to the geogrid type, foundation thickness and subgrade stiffness?"*

This question is divided in six sub-questions:

1. *How can an alternative Dutch design method based on the modulus improvement factor and using United States Army Corps of Engineers research be made?*

2. *How can the modulus improvement factor of a TriAx stabilised granular layer in asphalt pavements be determined Mechanistic-Empirically?*

3. *What is the influence of the type of geogrid?*

4. *What is the influence of the foundation thickness?*

5. *What is the influence of the subgrade stiffness?*

6. *How does the new method to determine the modulus improvement factor work out in a practical case?*

1.3. Objective

The goal of this study is to develop a new mechanistic-empirical method for calculating the effect of stabilising the base layer of asphalt paved roads with Tensar's TriAx geogrids. With respect to this objective a couple requirements are set out, to which the model should suffice. The requirements are that the model can calculate the influence of the geogrid type, foundation thickness and subgrade stiffness. Furthermore, this method will be based on the modulus improvement factor (MIF). Once a method has been developed, it will be applied in a project case to determine it practicality.

1.4. Scope

The project will be limited to the use of Tensar TriAx geogrids in the foundation of paved roads. Other geogrid types, like the BiAx or UniAx, or different application scenarios, such as unpaved roads or crane platforms, fall outside the scope of this study. The data used to create an improved model is obtained from research that made full scale test setups, to eliminate the need for scale factors.

Although research results and other sources used in this report came from other countries, all the work that has been carried out complies with the Dutch road design standards (eurocodes).

The research concerns a literature review of the available data from studies that have already been carried out. Optimization of the calculation model will be aimed at improving the foundation calculation but also take social, environmental or economic effects into consideration when required.

2. Theoretical framework

A new calculation model can only be built on a solid theoretical bases of current standard calculation methods. This part of the study starts with an explanation of the fundamentals of mechanistic-empirical pavement and the role and function of geogrids. This is followed by a comprehensive description of common pavement structure design methods and calculation models.

2.1. Load distribution

Roads are build-up of pavement and foundation layers that have as primary function to spread or distribute the load of traffic passing over it, so that the subgrade doesn't collapse. Van Gurp, van Vilsteren, van der Wegen & Hofstra (2014) explain that for unbound granular material the stability/stiffness, bearing capacity and load distributing ability are derived from the interlock at the area of contact between grains, as shown in Figure 4. The quality of the interlock determines a layer's ability to absorb shear stress and to distribute load. A stiffer and more stable layer has a higher bearing capacity and greater resistance to permanent deformation. The stiffness of foundation material is expressed by its elastic modulus. The elastic modulus is the resultants of many factors, e.g. grain grading curve, compaction, grain size, grain strength, moisture content and age. It is one of the most important mechanical characteristics of a foundation layer and represents the load distribution ability or its contribution to the bearing capacity.

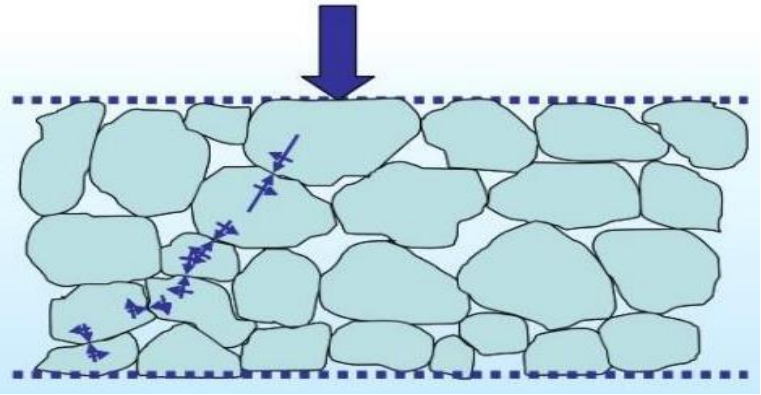

Figure 4: load distribution in a granular layer (Van Gurp et al., 2014)

The effect that including a geogrid in an aggregate layer has on the load distribution angle, the deformation and the bearing capacity is shown below in Figure 5 and Figure 6. In these figures the deformation is indicated by the white area. The load distribution is marked by the orange dotted line and the bearing capacity is marked by the orange block above the surface. In figure 5, the bearing capacity is 35kN, the load distribution is steep, and the deformation reaches deep into the foundation. In figure 6 the black dashed lines indicate the location of the geogrids. The insertion of the geogrid results in an increased bearing capacity of 49kN. The orange lines in figure 6 are wider than the orange lines in figure 5, indicating that the load distribution has increased. Finally, a decrease in the deepness of the deformation can be seen, as the area reaching in the foundation is lighter.

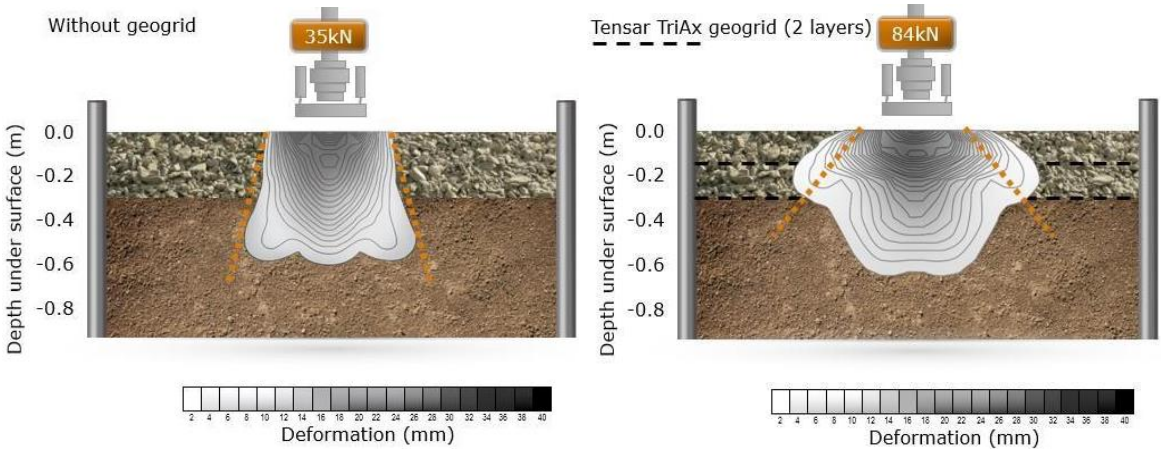

Figure 5 and Figure 6: show the effect of geogrid stabilisation on the bearing capacity, load distribution angle and deformation of a foundation layer (Kuljanski, 2016)

2.1.1. Failure Mechanisms

Roads can fail in a number of ways. To understand the benefits and function of foundation reinforcement or stabilisation, it is important to first gain insight into failure mechanics of paved roads and their foundation, also referred to as pavement structure/system. The CROW lists several failure mechanisms of paved roads in their publication 341 (van Gurp, van Vilsteren, van der Wegen & Hofstra, 2014):

- Elastic deformation
- Permanent deformation
- Cracking due to mechanical stress
- Shrinkage and hydration cracks
- Volume increase

Relevant to this study are the failure mechanisms of permanent deformation and cracking due to mechanical stress. Both failure mechanisms calculate with an exceedance of the maximum allowable stress and strain of the material used in a pavement layer (van Gurp, van Vilsteren, van der Wegen & Hofstra, 2014).

Structural rutting or deformation of the whole pavement system are two common forms of permanent deformation. It is caused by an excess of compressive vertical strain (ε_v) at the top of the subgrade. Fatigue cracking is a common form of cracking due to mechanical stress. It is caused by an excess of transverse tensile strain (ε_t) at the bottom of the lowest asphalt layer, which causes cracks to form there and grow further towards the top of the layer with each new axle load pass, as shown in Figure 7 (van Gurp, van Vilsteren, van der Wegen & Hofstra, 2014).

The impact of both failure mechanisms can be reduced substantially by including a geogrid to reinforce or stabilise the pavement system. This report focuses on stabilisation of the base by including a geogrid to reduce permanent deformation. How this can be done is explained in the following chapters.

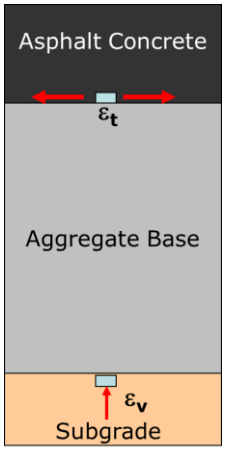

Figure 7: Horizontal and vertical strain on a pavement system while under load (Kuljanski, 2016)

2.2. How do geogrids work?

CROW publication 157 explains that in the case of using geogrids as road foundation reinforcement, a distinction is made between the function of *reinforcement* and the function of *mechanical stabilisation* (van Gurp, de Bruijn & van Putten, 2002). The terms reinforcement and stabilisation are in practice often used interchangeably and this can cause confusion when discussing the client's requirements in a project. It is important to note that *reinforcement* and *mechanical stabilisation* are not the same function and that they require different performance characteristics, different design methods and different forms of specification. This difference in function has been officially recognized by the European Organisation for Technical Approvals (EOTA) which acts on the authority of the European Commission.

This study focuses on the mechanical stabilisation. However, in order to understand the difference, the reinforcement factor will be explained briefly.

2.2.1. Reinforcement

In the function of reinforcement, the effect of a geogrid is often referred to as the membrane effect. For the membrane effect the geogrid contributes to the carrying capacity of the entire pavement structure, by exercising a horizontal tensile force coupled with a certain amount of vertical displacement, as shown by Figure 8. The geogrid must also have an embedment (or anchorage) length outside of the loaded zone. When building on soil with a low bearing capacity this vertical displacement must occur first, in order to activate the strengthening horizontal tensile forces (Tensar, 2018).

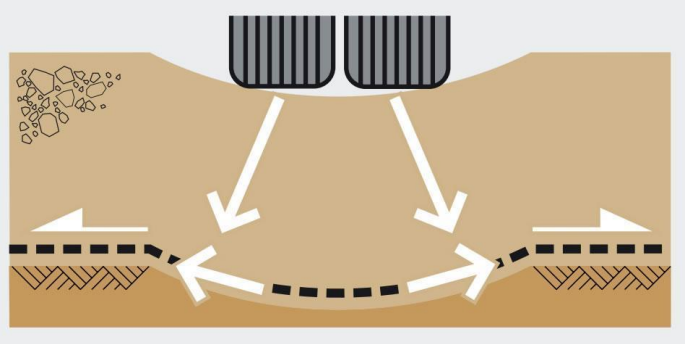

Figure 8: membrane effect and the reinforcement function (Tensar, 2018)

The vertical displacement required to generate these tensile forces is usually larger than the maximum allowable deformation of most pavement materials in permanently paved roads. Furthermore, deformation of the subgrade can negatively affect the stability of a road when the un-tensioned section of the geogrid is loaded or due to saturation and softening of the subgrade when ruts in the subgrade fill with water, as is mentioned in (Tensar, 2018).

2.2.2. Mechanical Stabilisation and Interlock

In the function of mechanical stabilisation, a geogrid is included to stabilise the foundation layer by increasing its soil stiffness. Vega, Kwast & van Gurp (2017) explain that the main effect of mechanical stabilisation consists of improved confinement of the aggregate particles and limitation of the lateral movement by a good interlock of the mineral aggregate in the apertures of the geogrid, as shown in Figure 10. Minimizing particle movement makes the whole pavement structure react stiffer and reduces deformation under applied loads. The lateral restraint of aggregate particles through interlock by a TriAx geogrid is shown in Figure 9. One study quantifying the ability of TriAx geogrids to laterally and vertically confine or interlock aggregate particle is (Huang, Tong, Shushu & Kwon, 2016). This study shows that there is significantly less vertical and horizontal displacement and less rotational movement of soil particles in foundation layer that has been stabilised by a TriAx geogrid versus the non-stabilised control layer during repeated loading. A selection of the results of the SmartRock paper from Pennstate University is given in appendix A.

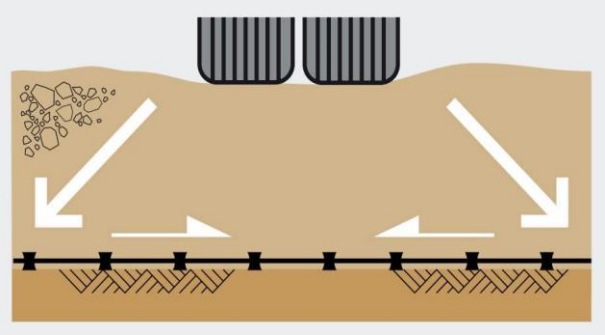

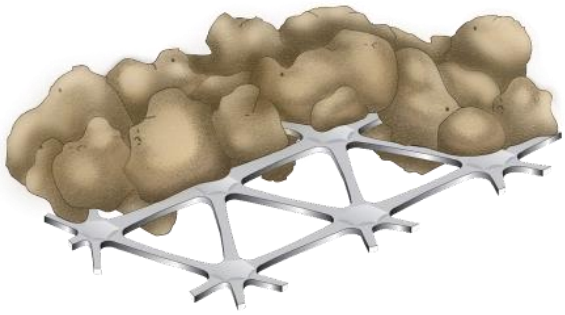

Figure 9: (left) stabilisation function (Tensar, 2018) and Figure 10: interlock of particles by a hexagonal geogrid (Tensar, 2018)

Mechanical stabilisation of a foundation layer can only occur if a geogrid performs under very low strain (maximum of 0,5% in the weakest direction of the geogrid according to Tensar design requirements), has a high radial stiffness and is dimensionally stable, e.g. retains its shape under load. In contrast to the reinforcement function and membrane effect, a geogrid adhering to the stabilisation function does not require vertical deformation to develop tensile forces, which would be undesirable when designing pavements.

Tensar TriAx geogrids work based on mechanical stabilization, as defined by the ISO Technical Committee TC 221 Working Group WG2 in the new ISO 10318 standard. They list the following effects of stabilising a foundation layer in (Kuljanski, 2018):

- Increased resistance to lateral shear of the foundation material due to heavy axle loads on the surface;
- Improved confinement of the foundation material, whereby the horizontal support stress in this layer increases, which subsequently results in a greater stiffness modulus;
- An improved distribution of stresses over the subgrade that generally leads to a higher stiffness modulus of the subgrade;
- A reduction of the shear stresses at the top of the subgrade, which results in a lower vertical displacement in the subgrade, resulting in a lower permanent distortion.

2.2.3. Influence of stabilisation over height

The extent to which a geogrid can stabilise a foundation layer depends on how well it can interlock the soil particles that lay on top of it. This is different for each combination of geogrid type and soil type. The spread of particle sizes within an aggregate grade is one of the primary factors for selecting the appropriate type of TriAx geogrid to use (Tensar, 2017). In practise this means that geogrids with shorter ribs and smaller apertures are used to stabilise layers with a smaller maximum particle size and geogrids with longer ribs and large apertures are used to stabilise layers with a larger maximum particle size, such as railway track ballast.

However, the stabilising effect of a geogrid is not felt throughout the whole soil layer. Instead the effect is limited to a certain range where the particles are first fully confined (e.g. fully interlocked), followed by a transition zone where the confinement is partial and decreasing to the point where influence of the geogrid is no longer felt and the unconfined zone begins, as shown by figure 11 below. This layer of (partially) confined soil is called the Mechanically Stabilised Layer (MSL). For Tensar TriAx geogrids, the standard values are that the fully confined zone is from 0,0cm to 15,0cm above the geogrid and the partially confined zone from 15,0cm to 40,0cm. For other geogrids, the confinement zone heights can be calculated from the largest grain diameter of the aggregate in which the geogrid is placed and the stiffness or shape-retaining characteristics of the product (Vega, Kwast & van Gurp, 2017).

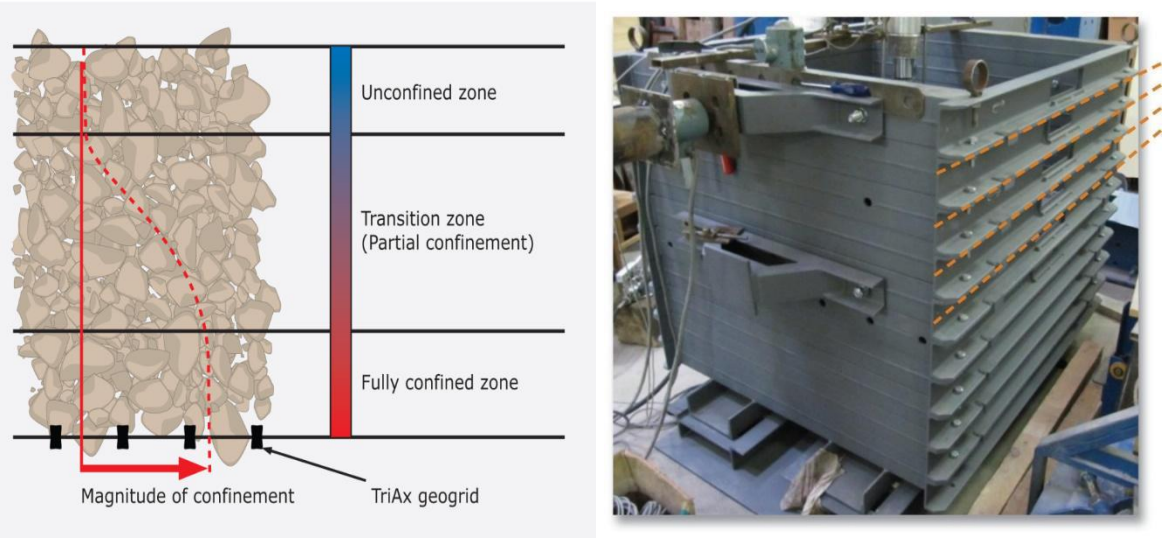

Figure 11: (left) transition of confinement of particles above a stabilising geogrid (Kuljanski, 2016) and Figure 12: shear box test setup with orange shear lines indicating shear planes (Tóth, Koren, Horvát & Fischer, 2012)

Researchers of Györ University concluded that “inner shear resistance can be determined as a function of distance from the geogrid layer” (Tóth, Koren, Horvát & Fischer, 2012). Figure 12 shows the test setup of a multi-level shear box with sectioned walls that can slide over each other, applying shear pressure on the grains within. By measuring the shear resistance at different distances from the geogrid, the function of pressure over distance shown in Figure 11 was found. Combining the results of previously mentioned SmartRock study with those of Györ University, it paints a clear picture of the significant stabilising effect a geogrid has on surrounding aggregate particles.

2.3. Improvement Factors

Common factors for quantifying improvement to a structure are required when comparing research and test results from different studies, application scenarios or countries. This study sets out three commonly used factors. The modulus improvement factor (MIF) is the most important of these factors. This factor quantifies the benefits of a stabilising geogrid. It is derived from the change in stiffness of a foundation layer, due to the inclusion of a stabilising geogrid.

Two other commonly used factors for quantifying the improvement made to road structure by including a geogrid are the Support Improvement Factor (SIF) and Traffic Benefit Ratio (TBR). Each factor gives a value to the difference between the standard non-stabilised road section and the new stabilised one.

2.3.1. Modulus Improvement Factor

The stiffness of an unstabilised granular layer depends on its thickness and on the bearing capacity of the underlying medium. An increase in stiffness of the underlying layers or an increase in bearing capacity of the subgrade, both lead to an increased stiffness of the base layer. When a geogrid is used to stabilise a foundation layer, the main factors determining its Modulus Improvement Factor are: (1) the type of soil/aggregate in which it is placed, (2) the layer thickness and (3) the type of geogrid (Vega, Kwast & van Gurp, 2017).

For example, when a geogrid used to stabilise the subgrade has a MIF = 3, the maximum stiffness of the subgrade, over the effective stabilising height of the geogrid, is equal to three times the stiffness of the mineral aggregate in the unstabilised situation.

The Modulus Improvement Factor is determined from-scale trafficking tests, and is calculated as follows (Vega, Kwast & van Gurp, 2017):

$$MIF = \frac{E_{2w}}{E_{2o}}$$

Where:

E_{2w} = Stiffness modulus of the reinforced foundation [MPa]

E_{2o} = Stiffness modulus of un-reinforced foundation [MPa]

Figure 13 shows an example of an unpaved road to clarify the relation between soil stiffness, layer thickness, bearing capacity, SIF and MIF.

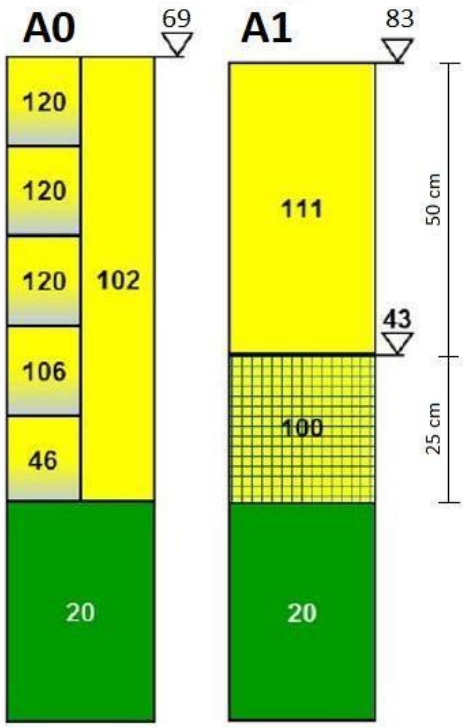

Figure 13: bearing capacity and elastic modulus of foundation and subgrade layer, demonstration the stabilising effect of a geogrid (Vega, Kwast & van Gurp, 2017)

This example of an unpaved road has a weak subgrade with a stiffness modulus of 20 MPa and 75 cm of sand subgrade, with a maximum stiffness modulus of 120 MPa. Situation A1 is stabilised by a geogrid with an effective stabilisation height of 25 cm, at the bottom of the subgrade. The triangle indicates the equivalent stiffness modulus of the underlying foundation at that particular height. A0 shows the division of the stiffness modulus per sub-layer of sand on the left and the average stiffness modulus of the entire sand layer on the right, according to the Austroads calculation model.

The manufacturer has specified that for this geogrid the SIF = 5 and the MIF = 3. The maximum stiffness of the stabilised part of the subgrade equals 5 x 20 = 100 MPa according to the SIF and 3 x 102 = 306 MPa according to the MIF. The lowest stiffness of 100 MPa (SIF) is decisive in this example. The effect of including a geogrid is an increased dynamic stiffness modulus at the top of the subgrade (increasing from 69 MPa for the unreinforced section to 83 MPa for the reinforced or stabilised section) and indicates an increase in bearing capacity.

2.3.2. Support Improvement Factor

The strengthening effect of foundation reinforcement or stabilisation depends not only on the characteristics of the geogrid, but also on the mineral aggregate in which it is applied, as well as on the structural layer in which it is placed. The Austroads design method clearly shows that there are limits to the stiffness of a granular layer. Those limits depend on the layer thickness and stiffness of the layer on top of which the granular layer is placed (Austroads, 2012). The same principle applies to granular layers with foundation reinforcement or stabilisation. The relative increase in stiffness of a reinforced granular layer will be larger. However, here too there are limits. The maximum improvement factor of the reinforced layer relative to the underlying layer is designated as SIF.

If, for a geogrid in the sub-base, the Support Improvement Factor = 5, then the maximum stiffness of the sub-base over the effective stabilising height of the geogrid is equal to five times the stiffness of the underlying subsoil layer.

The Support Improvement Factor is derived from full-scale trafficking tests and is calculated as follows (Vega, Kwast & van Gurp, 2017):

$$SIF = \frac{E_{2w}}{E_{4o}}$$

Where:

E_{2w} = Stiffness modulus of the reinforced foundation [MPa]

E_{4o} = Stiffness modulus of un-reinforced subgrade [MPa]

2.3.3. Traffic Benefit Ratio

The MIF and SIF quantify the structural improvement of a foundation, caused by including a geogrid (in a paved road). The Traffic Benefit Ratio (TBR) is different. It shows the relation between the amount of load repetitions a stabilised or unstabilised road can sustain, before a certain rut depth occurs. The TBR measures the difference in performance of the complete (unpaved) road structure, caused by including a geogrid in its foundation. It does not quantify the effect a geogrid has on the strength of individual foundation layers.

The Traffic Benefit Ratio is derived from full-scale trafficking tests and is calculated as follows (Vega, Kwast & van Gurp, 2017):

$$TBR = \frac{N_w}{N_o}$$

Where:

N_w = Number of Equivalent Standard Axle Loads (ESAL) passes over a reinforced road section [-]

N_o = Number of Equivalent Standard Axle Loads (ESAL) passes over an unreinforced road section [-]

Figure 14 shows the relation between rut depth and the number of load repetitions over a reinforced and unreinforced test section. The test section is considered to have failed when rut depth reaches 20 mm. In this example, the TBR is equal to 4400 / 400 = 11. This means that the unpaved road with the same thickness can handle a factor of 11 times more traffic, before reaching the same rut depth.

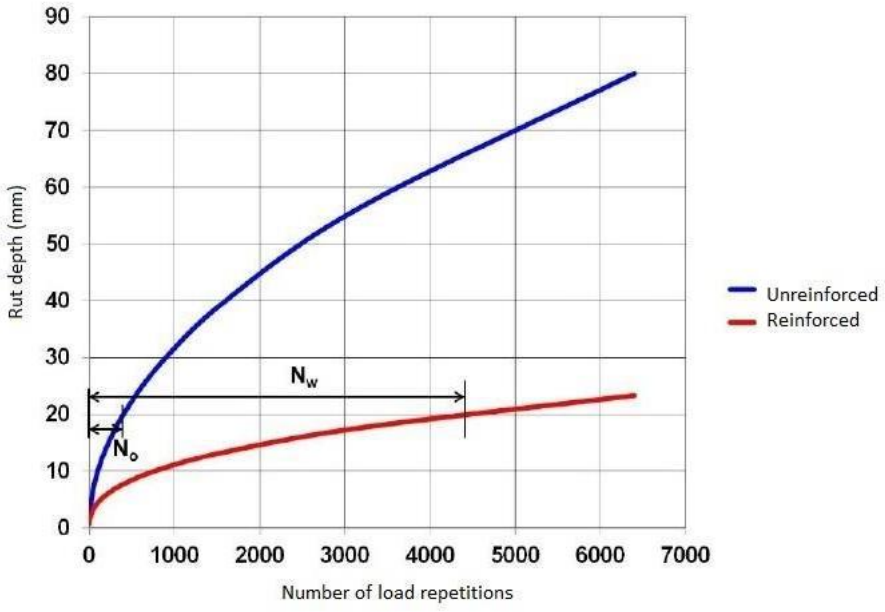

Figure 14: calculating the traffic benefit ratio from the difference in load repetitions at a certain rut depth (Vega, Kwast & van Gurp, 2017)

2.4. Pavement Design

Pavement design can be defined as "...the engineering discipline that ensures that the pavement system can provide an adequate level of service while sustaining the traffic loading for the duration of the design period" (Modelling and Analysis Systems, 2005). From this definition, three key concepts can be deduced: the serviceability, the pavement system and the traffic loading.

The serviceability describes the quality of the pavement as experienced by road users or as a description of the terminal pavement layer condition. The required level of service is often dictated by the road type or category and is a measure for the required design reliability.

The pavement system of a road consists of its constructed layers and the subgrade below. The main function of the pavement system is to offer enough structural load spreading capacity so that the applied stress on the subgrade stays within acceptable limits and does not cause deformation. This, while maintaining structural integrity in each individual layer.

The traffic loading quantifies the intensity of all traffic types over the design life of the pavement system. It is a spectrum and consist of a variety of vehicle types and axle loadings. When calculating the load on a pavement system the concept of load equivalency is used to convert a traffic spectrum into a single number of cumulative axle load passages, known as the Equivalent Standard Axle Load (ESAL).

Earlier pavement design methods like the California Bearing Ratio (CBR), the cover design method (Davis, 1949) and the American Association of State Highway and Transportation Officials (AASHTO) guidelines (1986), were mainly aimed at protecting the underlying subgrade. They did this by spreading the traffic load, so that no excessive deformation would occur. However, they did not allow for evaluation of the individual layers of the pavement structure for failure or deformation. They also could not predict the influence of repeated loading and the exposure to climate. Furthermore, these older models did not account for the use of geogrids in paved roads.

There are countries were the road design process is split between a geotechnical engineer and a pavement design engineer. The geotechnical engineer works on the road foundation, from the subgrade to the top of aggregate base layer. The pavement design engineer works on the asphalt layers, from asphalt base to surface. This division makes it difficult to incorporate the effect a geogrid placed in a foundation layer has on the asphalt layers and on the three concepts of serviceability, pavement system and traffic loading.

The Mechanistic-Empirical Pavement Design Method considers all three concepts of pavement design. It allows the effect of geogrid stabilisation to be calculated for every single layer, from subgrade to asphalt, for each of the three concepts. The Dutch design standard as well as the South African Mechanistic Design Method (SAMDM) and the newer AASHTO design standards all follow the Mechanistic-Empirical Principal.

2.4.1. Mechanistic-Empirical Pavement Design Method

The Mechanistic-Empirical Pavement Design Method (M-E) can evaluate the potential for failure in all pavement and foundation layers individually. Besides evaluating the potential for failure, the M-E can also be used to determine *how* the layers will fail, as well as to calculate the stresses and strains acting on a specific point within each layer. Furthermore, it is currently the most advanced design method used worldwide. M-E works like a two staged rocket. First the occurring strain is predicted with the help of a mechanistic linear elastic model. Secondly, this predicted strain is then used as input to determine the amount of available axle load transition with region-specific strain transfer functions.

The mechanistic part of M-E consists of linear elastic calculations. As Kuljanski (2016) explains in his report, a linear elastic model can calculate the stress, strain and deflection that result from a single, dual or tandem wheel load being applied, at any point in a pavement structure. The linear elastic model assumes that every pavement layer is homogeneous, isotropic and linearly elastic, and that every layer has an elastic modulus (E), Poisson ratio (v) and thickness. An alternative to the linear elastic model is the finite element method (You & Buttlar, 2014). However, this will not be further discussed.

The Empirical part of M-E is based upon full scale laboratory tests and project monitoring results of the behaviour of different pavement systems and road sections. It computes the fact that pavement material cannot absorb stress and strain indefinitely and that it will eventually be considered to have failed. Common causes for failure are fatigue cracks or deformation, i.e. rutting. The amount of Equivalent Standard Axle Loads (ESAL) needed to reach the point just before failure, also referred to as the limit state, is known as the design life. The design life of pavement material is calculated with equations called Transfer Functions. Transfer functions are used to calculate how long a material will perform satisfactory at a given stress-strain level. In other words; the number of ESAL's a pavement layer can withstand before it starts to deform or crack more than allowed by the serviceability limit. A simplified form of the standard M-E design method without geogrid is shown in Figure 15 below.

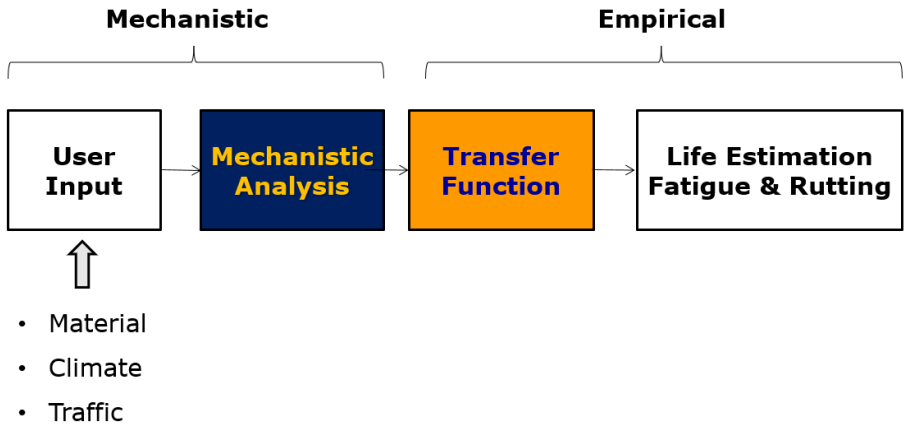

Figure 15: schematisation of the mechanistic empirical pavement design method (Kuljanski, 2016)

When a geogrid is introduced to stabilise the foundation layers, the M-E procedure must be altered to include the effects a geogrid has on the pavement system. There are two steps by which this is done, namely: the mechanical step and the empirical step (Marzurowski, Buckley & Kawalec, 2019).

Including the effect of geogrid stabilisation in the mechanical step can be made by introducing the modulus enhancement factor. The modulus enhancement factor demonstrates the immediate effect a geogrid has on the stiffness of a granular layer (Note that the modulus enhancement factor is not the same as the earlier mentioned MIF). This factor determines how much the stiffness of the layer may be increased, as a result of including a geogrid (Marzurowski, Buckley & Kawalec, 2019). This modulus enhancement factor is influenced by interlock and confinement. Better interlock and confinement entail a higher stiffness. The interlock and confinement decrease as the distance to the geogrid grows. The MSL formula uses the course of the stiffness to calculate the modulus enhancement factor for the entire granular layer (see Figure 11).

The formula used to calculate the modulus enhancement factor of the MSL is (Kuljanski, 2016):

This function falls under the intellectual property of Tensar.

For access to this function please send your request to:

info@tensar.nl

Calculating with stiffness retainment and Shift Factors is done in the Empirical step of the M-E design method, to include the effect of geogrid stabilisation. Shift Factors compute the stiffness retention of granular layers and asphalt (Marzurowski, Buckley & Kawalec, 2019). A geogrid does not only increase a layer's stiffness, it also helps a layer to retain this stiffness over a longer period of time. Figure 16 shows how the Shift Factor retains the stiffness of the pavement

structure, as it is subjected to more load repetitions, increasing the pavement life. The black curve represents the stiffness of the unstabilised layer. The orange curve represents the stiffness of the stabilised layer. The difference between the black curve and the orange curve, indicated by the grey arrow, is the shift factor.

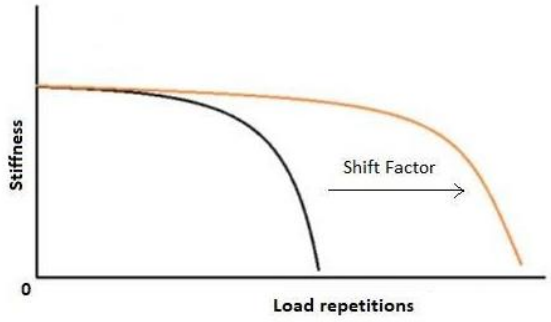

Figure 16: stiffness retention and shift factor (Kuljanksi, 2016)

There are two types of shift factors. The function below is used to calculate the shift factor for asphalt performance. The other function calculates the shift factor for the subgrade, but is not relevant for this study (Kuljanski, 2016).

This function falls under the intellectual property of Tensar.

For access to this function please send your request to:

info@tensar.nl

So as can be seen in the formula, the shift factor depends on the thickness of unbound granular layer (T_{abc}), the thickness of the asphalt layer (T_{ac}) and the distance from the bottom of the asphalt to the geogrid (D).

Figure 17 below, shows an example of a complete M-E design process. Every *column* defines a different (sub)step of the process. The first four *columns* are part of the mechanistic step. The last three *columns* are part of the empirical step. The red boxes show where in the process the MSL and shift factor functions can be included, to quantify the effect of geogrid stabilisation.

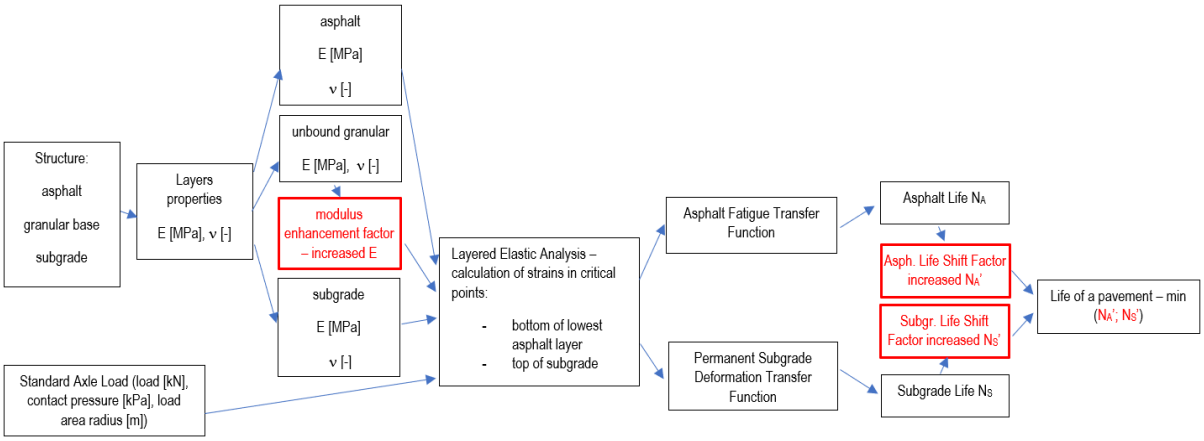

Figure 17: schematisation of the modified (red) mechanistic empirical pavement design method (Marzurowski, Buckley & Kawalec, 2019)

Another function with which the empirical step can be carried out is the strain transfer function which comes from 'Ontwerpinstrumentarium Asfaltverhardingen' (OIA). This function is referred to as the 'OIA' function and is stated below (CROW, 2014):

$$ln\left(N_{fkar}\right) = C_1 + C_5 * \left(ln\left(\varepsilon_{asf}\right) + C_2 * ln^2\left(E_{asf}\right) + C_3 * ln\, ln\left(E_{asf}\right) + C_4\right)^2$$

Where:

N_{fkar} = Characteristic fatigue strength asphalt, depending on strain level and asphalt stiffness [-]

ε_{asf} = Strain in asphalt [µm/m]

C_1 = $-(b^2 - 4ac)/(4a)$ [-]

C_2 = -0,064449 [-]

C_3 = 1,404363 [-]

C_4 = $b/(2a) - C_2 * \ln^2(S_{20°C,\,30Hz}) - C_3 * \ln(S_{20°C,\,30Hz})$ [-]

C_5 = a [-]

E_{asf} = Elastic modulus asphalt [MPa]

The values of a, b, and c are obtained from the fatigue line of the (reference) asphalt. The C factors are dependent upon the type of asphalt used in the system; they represent the Shift Factors mentioned earlier. This function requires calibration based on laboratory and full-scale tests. In his report, Lee (2017), highlights the importance of these tests and recommends Accelerated Pavement Testing (APT) for gathering the information needed to develop the Shift Factors.

2.4.2. Pavement Optimisation

Including a stabilising geogrid to a pavement structure changes how it reacts when subjected to load. It changes the occurring stresses, strains and deformations and increases the elastic modulus and pavement life. All these changes bring two major benefits to the design of a stabilised pavement system of which one or both can be utilised. The benefits are: (1) an increased design life and/or (2) a reduced thickness of the pavement system. Figure 18 shows an example of different design options utilising the benefits of geogrid stabilisation.

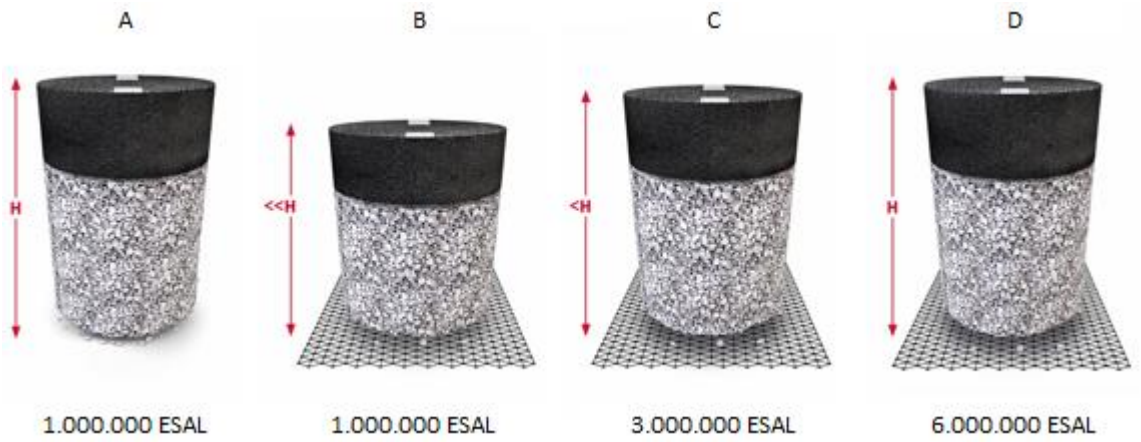

Figure 18: different alternatives for pavement optimisation (Tensar, 2016)

- Option A represents a standard unstabilised road section, that has an asphalt layer on top of a mineral aggregate foundation layer. It has a total height of H and a design life of 1.000.000 (one million) Equivalent Standard Axle Loads.
- Option B is stabilised by a geogrid at the bottom of the foundation layer and this allows for significant reduction of asphalt and aggregate layer thickness. This results in much lower construction cost, because it requires less excavation and less construction materials, while maintaining the design life of variant A.
- Option C utilises both stabilisation benefits. The thickness of the pavement system is reduced enough to cover the expenses of the geogrid but not more, so that part of the stabilising effect can still be used to increase the design life. Depending on the specific project requirements, the ratio between cost saving and increased performance can vary.
- Option D has the same pavement structure as variant A, but with a significantly increased design life. The (initial) construction costs of this variant are the highest of the four. This is due to the inclusion of the geogrid and the material cost. However, the relative costs over the entire period of use are the lowest of the four.

The process of changing the pavement structure and design life of a road due to the stabilising effect of a geogrid, is called Pavement Optimisation. It can be defined as “the design of flexible pavement to allow for reduction of thickness of layers, including asphalt layers, while maintaining the pavement life or increasing the pavement life while maintaining its thickness or a combination of both” (Marzurowski, Buckley & Kawalec, 2019).

2.5 Summary

This chapter was divided into four parts. The first part covered the effects of load distribution, which in turn explain how roads can fail. In the second part, the effects of geogrids on the foundation layer were set out. Geogrids have two main effects; reinforcement and stabilisation. This study focuses on the stabilisation effect. The effects of mechanical stabilisation and interlock are the key concepts in stabilisation. The third part covered the improvement factors, which can be used to quantify how much the foundation has been improved (MIF, SIF and TBR). The fourth part is the most important. This sets out the framework by which the analysis of this research is conducted. This framework is the M-E design process. This process consists of two steps; the mechanical and the empirical step. The mechanical step is made with linear elastic calculations. In calculating the effect of geogrid stabilisation, the MSL function fulfils an important role. Including the effect of geogrid stabilisation in the empirical step can be done with the SF function or the OIA function.

3. Methodology

This study developed a method to mechanistic-empirically calculated the MIF for asphalt paved roads. The previous chapter provided a framework from relevant literature and guidelines that were used to create this calculation method. A deductive qualitative literature review has been carried out. Hereto empirical data on the performance of geogrids has been compared. This chapter sets out how the data was gathered, as well as the research methods which were used to conduct this study. Subsequently, the creation and application of the new calculation method were demonstrated through a design application in a practical case. The created road design variants were analysed and compared with a life cycle cost analysis.

3.1 Data Collection

Chapter 2.4.1 explained the mechanistic empirical calculation method and described the function of the two parts. The mechanistic calculations in this study were done with the linear elastic calculation software called ERApave. ERApave calculates the occurring stress, strain and deformation after a passing single load, at a certain depth in a pavement structure layer. To do his, ERApave needs several input parameters from the soil properties and load characteristics. The empirical calculations in this study were done by using the OIA function. This section describes how these parameters were gathered, and the precise functioning and use of this software is explained in section 3.2.

3.1.1 USACE

The calculation method in this study is based on three phases of tests carried out by the United States Army Corps of Engineers (USACE) (Jersey & Tingle, 2010; Norwood & Tingle, 2014; Tingle, Jeremy Robinson & Norwood, 2017). These tests are full scale Accelerated Pavement Tests (APT), carried out with a Heavy Vehicle Simulator (HVS). These test sections, in the reports referred to as ‘test items’, were built and designed according to the American Association of State Highway and Transportation Officials (AASHTO) design guide. They consist of unstabilised and TriAx stabilised asphalt paved road sections, build on weak clay subgrades. All three reports plot the asphalt degradation results in a graph of rut depth (inch) over Equivalent Standard Axle Loads (ESAL) as can be seen in appendix C.

During the content analysis of the USACE reports, it became clear that there was missing data. The USACE phase 1 to 3 reports provided detailed information on the thickness and stiffness/modulus of the pavement structure’s layers, except for the asphalt. For the asphalt layers, only the thickness and type (Hot Mix Asphalt) were provided. The USACE reports designed and build their test sections according to AASHTO standards. TensarPave has three moduli. The program can be used to design according to the German Ev2 module, the Dutch unpaved road module (based on CROW 189 and 157) and the AASHTO module. Therefore, reconstructing the test sections in TensarPave, using the AASHTO module, should provide the same pavement structure characteristics as in the USACE reports. AASHTO uses a structural

number to indicate the strength of a layer. The stiffness (elastic modulus) can be derived from the structural number. Because the reconstructed test sections in TensarPave perfectly matched the test sections set out in the report, the missing stiffness of the asphalt layer could be derived from the reconstructed test sections in TensarPave. TensarPave reconstructions of all test sections are included in appendix E.

3.2 Calculation and Calibration

The data collected from the USACE reports was used as input for the mechanistic-empirical functions. The linear elastic calculation software and the OIA function had to be fitted to one another, in order to calculate the MIF of the USACE test sections. The process of fitting the linear elastic calculation software and the OIA function together will now be described.

3.2.1 Rut depth

The first factor that had to be determined was the rut depth. The rut depth is used as a benchmark throughout the calculation process. The American road design standards consider 0,50 inch to be the maximum allowable rut depth for high intensity roads, which is comparable to the serviceability limit of 1 cm rut depth on the asphalt surface layer often used in Dutch road design. ESAL's were read at 0,50 inch in the degradation curve of each item, to be used later in the OIA function. After determining the rut depth, the next step was to calculate the strain in the asphalt layer.

3.2.2 ERApave

Asphalt strain is calculated at the bottom millimetre of the asphalt layer, because the normative form of crack formation due to asphalt fatigue are bottom-up cracks. The asphalt strain also strongly depends on the stiffness of the base layer. The stiffness of the base layer can be increased by, among other things, including a stabilising TriAx geogrid. To calculate the occurring asphalt strain in the unstabilised test sections, all parameters listed under input in Table 1 had to be entered in the program. There were a total of six valid test sections (2B in red is not used) from which these parameters are retrieved. They will be referred to as shown in Table 2. The soil and output were test section specific characteristics. The load was the same for all test sections, except for test section 1B. 1B has a single axle instead of a tandem axle. 1B also has half the overall axle load, resulting in the effective load still being the same. The strain calculation results for the unstabilised test sections are shown below and the complete calculations be found in appendix G

- Strain = 353 um/m for 1B
- Strain = 240 um/m for 1C
- Strain = 153 um/m for 2A

ERApave parameters		
Input		Output
Soil	Load	
Thickness (cm)	Contact Pressure (kPa)	Stress: Szz, Sxx, Syy (kPa)
Modulus (MPa)	Axle Load (kN)	Deformation: wz (cm)
Poisson's Ratio (-)	Wheel Spacing (cm)	Strain: Ezz, Exx, Eyy (IE^-3)
Unit weight (kN/m^3)	Axle Configuration	
	Location: x, y, z (cm)	

Table 1: ERApave input parameters and results/output

USACE test sections			
Given name	From report	Item Nr.	Stabilised
1A	Phase 1	Item 1	Y
1B	Phase 1	Item 4	N
1C	Phase 1	Item 5	N
2A	Phase 2	Item 1	N
2B	Phase 2	Item 2	Y
3A	Phase 3	Item 1	Y
3B	Phase 3	Item 2	Y*

*Table 2: Name table with overview of all USACE test sections and reports (*section 3B is stabilised with a TX8 geogrid where all other sections are stabilised with TX5)*

3.2.3 OIA function

After the strain has been calculated in ERApave, representing the mechanistic part of the new model, the OIA function was put in excel and rearranged so that it would equal strain and the validity of the function was verified through iteration. The function below represents the empirical part of the new model.

$$\varepsilon_{asf} = e^{\frac{\sqrt{\ln(N_{fkar}) - C1}}{C5} - C2 * \ln(E_{asf})^2 - C3 * \ln(E_{asf}) - C4}$$

The next step was to fill in this function, starting with the asphalt stiffness that was acquired from the structural number (SN) of each pavement structure layer in the TensarPave models. For all test sections counts that:

- E_{asf} = 6500 MPa

The next factor is the N_{fkar} which shows the amount of ESAL's read from the degradation curve at 0,50 inch of each test section. The values in the USACE reports are given in 20 Kip (= 89 KN) ESAL's but the calculations are done with the Dutch standard of 100 KN ESAL and are calculated with the fourth power rule, as shown below:

- N_{fkar} = 4200 ESAL 20 Kip or 2646 ESAL 100 KN for 1B
- N_{fkar} = 16500 ESAL 20 Kip or 10397 ESAL 100 KN for 1C
- N_{fkar} = 500000 ESAL 20 Kip or 315047 ESAL 100 KN for 2A

The C factors were the last parameters that had to be filled in. The functions listed in chapter 2.4.1 to calculate the C factors were not unusable, because the resulting strain stayed far from the values calculated in ERApave. The correct C factors were eventually acquired from material specifications of a foundation base layer from project Waalwijk, included in the appendix F.

- C1 = 39,176585
- C2 = -0,064449
- C3 = 1,404363
- C4 = -1,058189
- C5 = -0,212611

Choosing the right C factors was critical to the calibration of the function and of the new model. The strain (ε_{asf}) calculated with the OIA function matched those calculated with ERApave within a margin of 15%, which is acceptable.

Calculated strain			
Nr.	Strain OIA (um/m)	Strain ERApave (um/m)	Difference (%)
1B	340	353	-3,7
1C	260	240	8,2
2A	130	130	-15,3

Table 3: calculate strain and percentage difference

After finding the correct C factors the function was calibrated and could be used in the next step to calculate the elastic modulus of the stabilised aggregate foundation layers in test sections 1A, 3A and 3B. Test section 2B had to disregarded for further calculations in this study because a temperature related failure occurred during the USACE test on this section, which compromised the integrity of the pavement structure and led to increased degradation, as shown in appendix C.

3.2.4 Stabilised sections

After calibrating the OIA function, it was used to calculate the strain for the stabilised test sections 1A, 3A and 3B. This was done by entering the amount of ESAL's (N_{fkar}) that were extrapolated from the degradation curves using the power rule to create a trend line for each test section, see appendix C. The American 20 Kip ESAL values were translated to European 100 KN ESAL values with the fourth power-rule. After that they were entered in the function to calculate the occurring strain (ε_{asf}), following the same process as for the unstabilised sections. The next step was to model these test sections in ERApave, again with test section specific soil and output values but the same load values. The major difference being that the elastic modulus of the stabilised base layer was unknown beforehand. The elastic modulus had to be increased incrementally until the resulting strain (closely) matched the strain from the OIA function.

Stabilised test section calculation values						
	OIA function			ERApave		
Nr.	ESAL 20 Kip	ESAL 100 KN	Strain (um/m)	Elastic Modulus (MPa)	Strain	MIF
1A	200000	126019	157	700	153	3,30
3A	7000000	4410656	73	1400	73	*
3B	8000000	5040750	71	1370	72	*

Table 4: Calculation values from stabilised test sections

By dividing the increased elastic modulus with that of another unstabilised test section that is otherwise identical, the MIF can be calculated. For section 1A this means dividing its elastic modulus of 700 MPa by the elastic modulus of 1B of 212 MPa to get a MIF of 3,30. Calculating the MIF based on identical stabilised and unstabilised test sections was not possible for sections 3A and 3B because an unstabilised opposite was not available. Consequently, the MIF cannot be calculated for these sections, which leaves the MIF of 3,30 from section 1A as the only datapoint to be used in further calculations. The lack of extra test sections from which the MIF can be calculated is a major shortcoming in the USACE reports that will be further discussed in chapter 4.

3.3 Mechanically Stabilised Layer and Shift Factor

After the MIF has been determined the individual influence of the geogrid type, foundation thickness and subgrade stiffness had to be calculated. This was done with a combination of Tensar's proprietary mechanically stabilised layer (MSL) and shift factor (SF) functions. As chapter 2.4.1 explained, these two functions quantify two ways in which the geogrid's effect can be described. Because the unconfined zone is not directly affected by the geogrid, the shift factor only increases the effect of the fully and partially confined zones.

This function falls under the intellectual property of Tensar.

For access to this function please send your request to:

info@tensar.nl

The result of incorporating the shift factor into the MSL function is shown above and will be referred to as the enhanced MSL function. The enhanced MSL function was calibrated for test section 1A with a MIF of 3,30, by changing the values for A and B. The ratio between A and B was set at 2,5 in accordance with previous internal studies carried out by Tensar. With the values shown in Table 5 the MIF of 3,30 was acquired.

Test section 1A							
MIF	input					result	
	Esg (psi)	Tabc (inch)	Tf (inch)	Tp (inch)	SF	A	B
3,30	4350	8,0	6,0	2,0	1,204	2,031	0,812

Table 5: Modified MSL function input, results and calibration

3.4 Designing variants

3.4.1 Design criteria

In order to be able to answer the final sub-question for application of the new model in a practical case, three stabilised and one unstabilised design variants had to be made for the project 'Reconstruction of the Kortenoord in the municipality Zuidplas. This road had to be rebuilt completely because the weak subgrade had caused subsidence and cracks severely damaging the road. The design criteria of the new road were:

- Minimum design life of 20 years
- Minimum of 4618444 ESAL of 100 kN

Other important design aspects are the construction cost, maintenance cost, cost over the total lifespan and CO2 emissions. Chapter 2.4.2 described three was to utilize the stabilisation benefits. First is to maximise the design life or the amount of ESAL a road can withstand (variant maximum). Second is to minimise the construction cost of the road, by reducing the asphalt and foundation layers (variant optimised). Third is to only save enough on construction cost to earn

back the cost of the geogrid and use the rest of the benefit to increase the design life (variant same cost). The difference between designs was made by variations in the asphalt layer thickness. The standard road design without geogrid stabilisation was also considered as a design variant.

3.4.2 Design calculations

The variants were designed with the new mechanistic-empirical design method, using the MIF of 3,30 as the only datapoint. The three stabilised and one unstabilised sections where modelled in ERApave to calculate the occurring strain at the bottom of the asphalt layer. All input data was acquired from the application proposal (Kuljanski, 2017) and the complete ERApave calculations are included in appendix G. The load characteristics for project Zuidplas were based on a traffic count carried out by the municipality. This resulted in an axle load spectrum instead of a fixed load and a combination of load factors had to be selected that best represented this spectrum.

- Axle configuration = Single axle/Dual wheels
- Contact Pressure = 800 kPa
- Axle Load = 70 kN
- Wheel Spacing = 50 cm

The calculated strain of each variant was then entered in the calibrated OIA function to get the amount of ESAL each design could absorb. The OIA function used the representative asphalt stiffness (E_{asf}) of the asphalt surface, binder and base course layers, as determined by (Kuljanski, 2017).

- E_{asf} = 5801 MPa

3.4.3 Comparing design variants

The four design variants (unstabilised standard, stabilised maximum, stabilised optimised and stabilised same cost) were compared through a comprehensive life cycle cost analysis (LCCA). They were also evaluated for common real-world scenarios or practises, that would give preference to a certain design. This preference could be caused by: budgetary planning, budget restrictions or unforeseen construction work. The LCCA calculations were divided into four main parts:

- Design life and traffic load.
- Unit costs.
- Life cycle and net present value.
- Environmental impact.

The design life and traffic load were calculated by combining the traffic count information with the calculated amount of ESAL for each variant. The traffic load was determined at 342 trucks per day in each driving direction, with a projected annual autonomous growth of 1,5%. Knowing the original designed ESAL amount over 20 years from Kuljanski (2017), the ESAL per truck

could be calculated, along with the lifespan (in years) of each variant. The calculated lifespan of the standard unstabilised variant was 19 years. This conflicts with the lifespan minimum of 20 years calculated in Kuljanski (2017). This error could be a result of different guidelines used in the calculations. The calculations in Kuljanski (2017) were made according to the AASHTO guidelines, where the calculation method developed in this study were made according to the Dutch CROW guidelines. Because a lifespan of 20 years is more reliable, and because using a lifespan of 19 years would lead to an inaccurate representation of this variant in the LCCA, the design life was determined at 20 years for further use (*).

The unit cost calculations were given in euro per square meter per centimetre (€ / m2*cm) and included the material cost and dimensions of each pavement system layer, along with the cost of maintenance. All listed prices include the cost of labour and were adjusted for inflation (GWW Kosten, 2018). The construction costs are built up of: the asphalt costs for the surface, the costs of the binder and base course, the gravel cost for the base layer, the sand cost for the sub-base and finally the cost of the geogrid. The maintenance costs include small yearly maintenance and renewal (removal plus construction) of the asphalt surface and binder layer every ten years. Reconstruction costs consist of removal of all the asphalt layers, excavation of the aggregate base layer and putting new layers back in place.

The life cycle cost is calculated by plotting all the applicable unit costs per year and calculating the net present value of these future expenses after a certain amount of years. The construction cost is applied once at year zero, the small maintenance cost is applied yearly, the asphalt surface maintenance is applied every ten years and reconstruction costs are applied when the design life of the respective variant is exceeded. Every year the net present value of the sum of the costs is calculated by adjusting it for inflation and a degradation in value of 2,5% per year (CPB, 2018).

The environmental impact of each variant was calculated with Tensar's proprietary Spectra Value Calculator software. Spectra Value Calculator expresses the environmental impact of the construction in kilogram CO2. Input parameters include the travel distance for materials and geogrids, project cost rates, project activity rates, several conversion factors and pavement structures dimensions. The CO2 usage for the construction of each variant is linked to its design life and is integrated into the LCCA.

4 Results

This chapter states the results of this study. It starts with a summary of the new mechanistic-empirical calculation method and the mechanistically stabilised layer function, followed by the pavement structure design variants and finally the results of the life cycle cost analysis.

4.2 Calculation method

The calculation method comprises of two parts. Part one is used to calculate the MIF. This part consists of a mechanistic-empirical design procedure. This M-E procedure is divided into two steps. The mechanic step is carried out by using ERApave. The empirical part is carried out by filling in values in the calibrated OIA function:

$$\varepsilon_{asf} = e^{\sqrt{\frac{\ln(N_{fkar}) - C1}{C5}} - C2 * \ln(E_{asf})^2 - C3 * \ln(E_{asf}) - C4}$$

This results in a MIF of 3,30.

The second part of the calculation method consists of equating the MIF to the enhanced MSL function:

This function falls under the intellectual property of Tensar.

For access to this function please send your request to:

info@tensar.nl

This will calibrate the enhanced MSL function. Entering a MIF value of 3,30 into this formula, a ratio between A and B of 2,5 has been calculated. Meaning that the enhanced MSL function needs to be calibrated on a ratio of 2,5 between A and B.

A = Range parameter to provide maximum enhancement in fully confined zone

B = Range parameter to provide maximum enhancement in partial confinement zone

With the enhanced MSL function the effect of geogrid type, foundation thickness and subgrade stiffness can be calculated. However, this requires data where one of these three factors have a determining role. Because there are no available data points, there are no results.

4.3 Road design variants

Using the MIF, derived from the first part of the new calculation model, four pavement structure variants for project Zuidplas were designed. The three stabilised variants have different thicknesses of asphalt layers which leads to savings in construction cost, to an increased design life or to a combination of the two. Variant 2 (maximum) has the same asphalt thickness as the unstabilised standard variant and uses the geogrid stabilisation effect solely to maximise the design life. This variant has the highest construction cost since the inclusion of a geogrid is not compensated by savings elsewhere. Variant 3 optimised meets the minimum required design life and has the lowest construction costs because the stabilising effect is solely used to reduce/optimise the pavement structure. Variant 4 same cost has approximately the same construction cost as the standard unstabilised variant 1 because the asphalt base layer is reduced by one centimetre to compensate for the cost in the geogrid. However, most of the stabilising effect is still used to increase the design life. The thickness of the mineral aggregate base layer and the sand sub-base layer were not changed for any variant. Figure 19 shows all four design variants A larger format of figure 19 is included in appendix H.

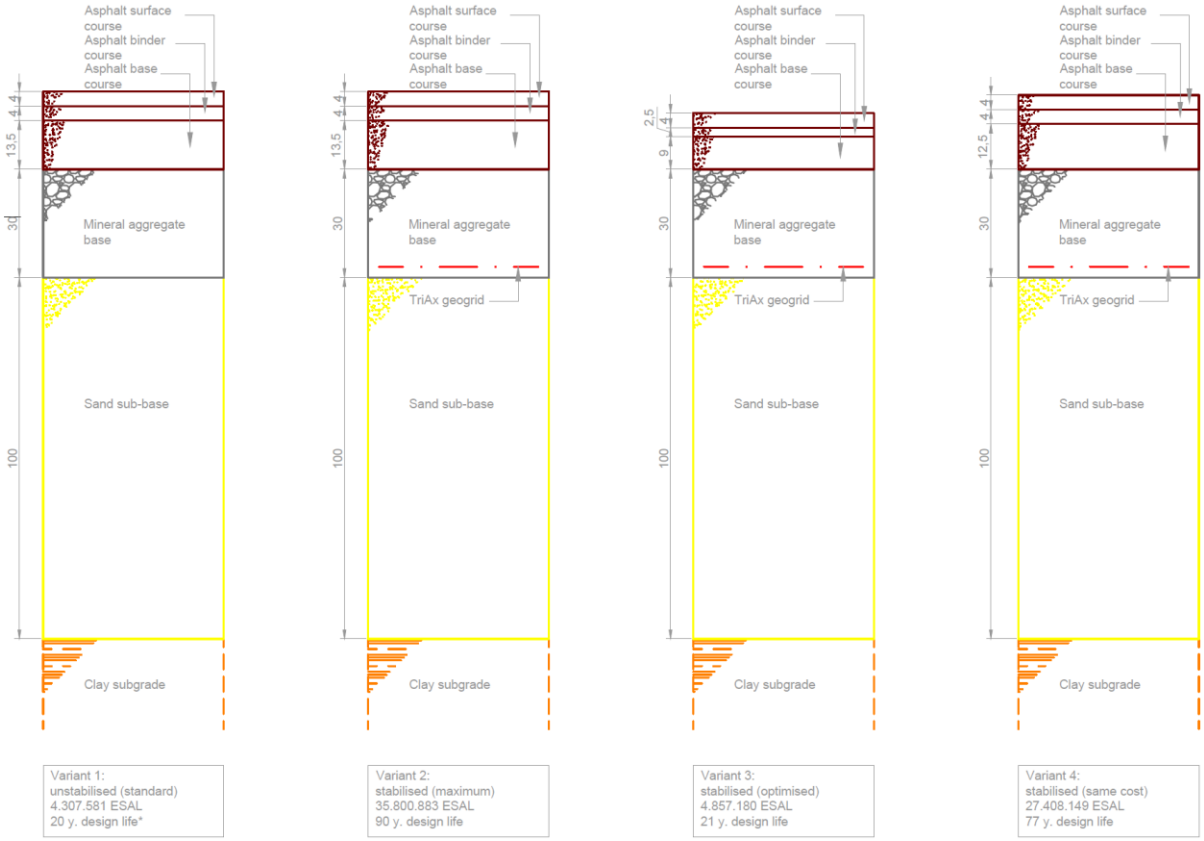

Figure 19: The four road design variants for project Zuidplas

4.4 Life cycle cost analysis

All four variants meet the project requirements but vary widely in initial construction and overall operating cost when a longer lifespan is considered. A life cycle cost analysis is a very useful tool to compare alternatives under these conditions and to select the alternative that is more cost-effective. Table 6 shows the net present value of each variant over a certain lifespan. This is the amount of money that must be set aside to construct, maintain and rebuild (if necessary) every variant over a certain number of years. Because the LCCA takes the residual value into account, variant 'maximum' is the most cost effective, albeit by a small margin. This advantage flips when a longer lifespan is considered because the inflation of 2,5% reduces the worth of the residual value over time. The reduction is larger than the increase in design life acquired from a more expensive pavement structure. Because the cost difference between the 'same cost' and 'maximum' variants is very small, a small change in inflation can tip the scale in the advantage of one or the other alternative. This must be kept in mind when reviewing the calculation results.

The difference in the costs between variants 1 and 4, and between variants 2 and 3 is in both cases roughly a factor of 1,25 at a lifespan of 20 years. At a lifespan of 25 years this factor has doubled to 2,5. This is due to the high costs involved with rebuilding the road, i.e. replacing the asphalt and mineral aggregate layers of the pavement structure.

Life Cycle Cost Analysis				
lifespan (years)	Net Present Value (€/m2)			
	1. unstabilised (standard)	2. stabilised (maximum)	3. stabilised (optimised)	4. Stabilised (same cost)
20	115,96	84,81	101,37	85,04
25	363,19	140,94	339,15	141,12
50	914,20	324,70	871,42	324,36
Estimated Design Life (years)				
	20,00	90,00	21,00	77,00

Table 6: life cycle cost analysis and design life of each variant (green is most favourable)

The stabilised variants have a lower net present value that the unstabilised variant, at any given lifespan. This indicates that there is a significant benefit to building a pavement structure with a stabilising geogrid. Including a geogrid does not have to increase the construction costs, but can lead to cost savings in construction and maintenance, while also increasing the lifespan of a road. Geogrid stabilisation can lead to a reduction in CO2 emissions during construction and reduce the negative impact on the environment. See the lower values of variants 2-4 in comparison to the values of variant 1.

Construction Cost and CO2 Emissions				
	1. unstabilised (standard)	2. stabilised (maximum)	3. stabilised (optimised)	4. stabilised (same cost)
Initial construction (€)	67,85	69,85	54,85	67,35
CO2 usage over 20 y. (KgCO2e)	828972	833283	769299	822589
CO2 usage over 25 y. (KgCO2e)	1657944	833283	1538598	822589
CO2 usage over 50 y. (KgCO2e)	2486916	833283	2307897	822589

Table 7: construction cost and CO2 emissions of each variant (green is most favourable)

5 Discussion

This chapter provides a discussion about the results. This will include an explanation of how to interpret the results. It also includes a reflection on the quality of this study.

5.1 Calculation method

The MIF has been determined mechanistic-empirically with the ERApave software program and the calibrated OIA function. The calculation results are in line with practise based expectations and can be used in the Dutch road design process because the calculation model follows Dutch road design guidelines. The first part (M-E) of the new calculation method resulted in a MIF of 3,30. This means that the maximum stiffness of the subgrade, over the effective stabilising height of the geogrid, is equal to 3,30 times the stiffness of the mineral aggregate in the unstabilised situation.

In order to determine the effect of geogrid type, soil thickness and subgrade two elements are required. First the enhanced MSL function needs to be (perfectly) calibrated. Secondly, there need to be available test sections in which one of these three factors play a determining factor. Using the MIF obtained in the first part, the enhanced MSL function was calibrated. However, this one calibration is the only datapoint, meaning that the enhanced MSL function is not perfectly calibrated. Also, there are no available data points where one of the three factors play a determining role. Therefore, the created calculation model has room for improvement. Besides the shortcoming in the model, it does offer a great starting point for further research. With more data, this model can be perfected.

There are two points of attention underlying the calculation model. First, the asphalt stiffness not being provided by the USACE reports. Second, the extrapolation of the amount of ESAL from the degradation curves of the stabilised test sections.

The USACE phase 1 to 3 reports provided detailed information on the thickness and stiffness of the pavement structure layers, except for the asphalt. With respect to the asphalt layer, only the thickness and type (Hot Mix Asphalt) were provided. The asphalt stiffness was derived from the structural number (SN) of the pavement structure layers in TensarPave. Thus, it could not be verified with the stiffness of the build test section's layers (Tensar, 2019). Although this way of back calculating the elastic modulus is valid, verification with the build test sections is preferable.

The amount of ESAL in the stabilised test section's degradation curves had to be extrapolated. This, because the rut depth of these sections had not reached the required 0,5 inch, before the end of the test. The degradation curves of stabilised roads from several other studies were carefully examined. In order to ensure the validity and reliability of the extrapolation of the ESAL's with an exponential trendline. Although the extrapolation was based on proper research, it still leaves room for a slight deviation.

It is important to state that the calculation method described is calibrated for foundations with a subgrade of 3% and 6% CBR and that this calculation method is not suited for use outside of the range of CBR values between 2% and 7%.

5.2 Enhanced MSL function

The enhanced MSL function is created by putting the SF and the MSL functions together. This enhanced MSL function needed to be calibrated. In this study, one datapoint (one MIF) was available to calibrate the enhanced MSL function with. A calibration based upon a sole datapoint is likely to be inaccurate. Therefore, the enhanced MSL function with, the calculated calibration values, is not suited to use in practice. However, the demonstrated way to calculate the enhanced MSL function does serve as a good foundation for future calibration. Future research should be aimed at collecting more data points.

5.3 Variants and LCCA

The road design variants and the LCCA clearly show the advantage of building with TriAx stabilising geogrids. The results in table 6 show that the net present value of the stabilized variants is always lower than the net present value of the unstabilised variant. Meaning that the amount of money that needs to be set aside, is lower. When looking at the construction costs, the stabilised maximum variant is the only variant that is more expensive than the unstabilised variant. Finally, the stabilised variants, same cost and maximum, lead to a major reduction in CO2 emissions during construction.

Because this calculation method was specifically created for asphalt paved roads and because Tensar wants to increase the use of pavement optimisation, the stabilising effect was only used to change the asphalt layers of the pavement system variants. It could also be used to change the mineral aggregate base or sand sub-base, but this would require a recalculation of the stiffness of all layers and of the stabilising effect. This would unnecessarily complicate the calculation. This could be a worthwhile option in scenarios where e.g. the weight of the pavement structure is an important factor, the water level stands close to the surface or contaminated soil requires a pavement structure with minimal excavation depth. Because this study focuses on geogrid stabilisation in asphalt paved roads and the practise of pavement optimisation, changing the asphalt layers is the best way to demonstrate practical use of this model.

As stated in the results, the difference in net present value between variant 2 (maximum) and variant 4 (same cost) are very small, see table 6. The percentage of inflation and value loss is the tipping point that decides which of the two variants has the lowest net present value. At the current 2,5%, variant 2 is cheaper when considering a 20 or 25 year lifespan. Variant 4 is cheaper at a 50 lifespan. If the inflation and residual value depreciation were increased to 3 %, variant 4 (same cost) would be cheaper at all lifespans. It is important to realize the sensitivity of the function so that the results are interpreted correctly. A detailed study into the residual value of roads, combined with an estimate of the inflation could bring closure to this problem.

5.4 Validity and reliability

Determining the MIF was based on multiple test sections from the USACE reports. There was a sufficient amount of data points available to build a model that could determine the MIF. Therefore, this contributes to the validity of this model.

The second part of the calculation used the MIF as input for determining the influence of the geogrid type, foundation thickness and subgrade stiffness. However, there were two shortcomings. First, in this study only one MIF could be calculated, meaning that only one datapoint was available. The validity of the results is negatively influenced by the lack of data points required for further calibration and optimisation of the calculation method. Second, because only one datapoint was available, a comparison between the results stemming from the calculation method could not be made. So, there are no valid results of the influence of geogrid type, foundation thickness and subgrade stiffness on the stabilised pavement structure.

This research uses existing calculation software and follows the widely used Dutch guideline by CROW and the American AASHTO. Following these guidelines contributes to the replicability of the results obtained in this study. Furthermore, every step of this research has been elaborately set out in the Methodology chapter. Therefore, following those steps, one would obtain the same results. In addition to the Methodology chapter, more extensive explanations are included in the appendices.

6 Conclusion and Recommendation

This study created a mechanistic-empirical calculation method to determine the modulus improvement factor of a stabilised granular base layer in asphalt paved roads. The new method has been applied in a practical case to design pavement structure variants and these variants were compared with a life cycle cost analysis. The central question of this research was:

"*What is the Modulus Improvement Factor of a with TriAx geogrids stabilised granular base layer for Mechanistic-Empirically designed asphalt pavements, in relation to the geogrid type, foundation thickness and subgrade stiffness?*"

This question was divided into six sub-questions. In order to provide an answer to the central question, the sub-questions will first be set out and answered separately.

The first sub-question was: "*How can an alternative Dutch design method based on the modulus improvement factor and using United States Army Corps of Engineers research be made?*"

Research shows that the mechanistic-empirical pavement design process is currently the most advanced method to design a pavement structure. M-E allows stiffness calculations of individual layers. It is therefore best suited to make a new calculation method based on the MIF.

The second sub-question was: "*How can the modulus improvement factor of a TriAx stabilised granular layer in asphalt pavements be determined Mechanistic-Empirically?*"

In order to mechanistic-empirically determine the MIF, two steps had to be carried out. In the first step the mechanistic calculations were done by the linear elastic software program ERApave. In the second step the empirical calculations were made with the strain transfer function from OIA. These two parts were fitted and calibrated so that they worked in tandem to calculate the MIF of TriAx stabilised granular layers in asphalt pavements.

The third, fourth and fifth sub-question are discussed together. These questions are about the influence of geogrid type, foundation thickness and subgrade stiffness, respectively, on the stabilised pavement structure. As discussed earlier, in order to provide an answer to these questions, a comparison had to be made between results where each of these factors fulfil a determining role. This comparison could not be made due to the lack of data points. Therefore, no answer to these sub-questions can be provided.

The sixth sub-question was: "*How does the new method to determine the modulus improvement factor work out in a practical case?"*

The new calculation method proved to be suited to calculate the MIF. As the results show, four variants for project Zuidplas were created. The usefulness of these variants was demonstrated in the LCCA. For example, when a governmental body writes a tender to build a new road the minimum lifespan and maximum costs are two very important design characteristics. Public tenders often have a strong preference for the cheapest alternative. The results show that using a LCCA to choose a design, instead of the initial construction costs, can lead to major savings over time. Although variant 3 (optimised) has much lower construction costs, when calculated for net present value it is not the cheapest option. The 'same cost' variant is interesting because its

initial construction cost is comparable to that of the unstabilised variant while having reducing CO2 emissions, lower life cycle cost and an increased design life.

Now to answer the research question: "*What is the Modulus Improvement Factor of a with TriAx geogrids stabilised granular base layer for Mechanistic-Empirically designed asphalt pavements, in relation to the geogrid type, foundation thickness and subgrade stiffness?*"

The MIF factor calculated in this study was MIF = 3,30. This was done by creating and subsequently calibrating a mechanistic-empirical calculation method. The influence on the pavement structure of the geogrid type, foundation thickness and subgrade stiffness could not be calculated. This, because a comparison between different datapoint could not be made, as explained in sub-questions 3 to 5.

6.1 Recommendations

To answer the third, fourth and fifth sub-question, and subsequently the main question, additional research is required. This additional research is necessary to further optimise, calibrate and validate the calculation method. It is very important that future studies are carried out identically to the USACE phase 1 to 3 studies (see Jersey et al., 2010; Norwood et al., 2014; Tingle et al., 2017). Preferably by the same institution to ensure conformity of results. Table 8 shows the test sections that were used during this study (see 1A until 3B). P1 to P4 are four proposed test sections for future research that would be most effective. These proposed test sections would create four new data points for calibration and optimisation of the calculation model. They would also create the possibility to compare between sections where the only variable is either the type of geogrid, foundation thickness or the subgrade stiffness (expressed in the California Bearing Ratio or CBR).

	Existing usable test sections						Proposed test sections			
	1A	1B	1C	2A	3A	3B	P1	P2	P3	P4
Stabilised (Y/N)	Y	N	N	N	Y	Y*	Y	Y	N	Y
Asphalt (cm)	5	5	7,5	10	7,5	7,5	7,5	10	7,5	7,5
Base layer (cm)	20	20	20	20	15	15	20	20	15	15
Subgrade (CBR)	3%	3%	3%	6%	6%	6%	3%	6%	6%	3%

*Table 8: Existing and proposed test section characteristics (*section 3B is stabilised with a TX8 geogrid, not TX5)*

A more general recommendation to clients of road design is to increase the use of life cycle cost analysis in the decision making process. This study gives a clear example of the value of analysing a structure on its life cycle cost in combination with its impact on the environment, instead of the initial construction costs.

7 Bibliography

American Association of State Highway and Transportation Officials. (1986). AASHTO guide for design of pavement structures, 1986. Washington, D.C: American Association of State Highway and Transportation Officials

Austroads. (2012). *Evolution of Guide to Pavement Technology Part 2.*

Castwright, M. (2014, September 17). Romans Roads. In *Ancient History Encyclopaedia.* Retrieved from https://www.ancient.eu/article/758/

CROW. (1994). *Gefundeerd op weg.* CROW media. Retrieved April 8, 2019

CROW. (2014). *Specificaties Ontwerp Asfaltverhardingen.* Dienst Grote Projecten en Onderhoud. CROW. Retrieved March 18, 2019, from https://www.crow.nl/thema-s/infratechniek/asfaltverharding/oia

Davis, E. H. (1949). The California Bearing Ratio Method for The Design of Flexible Roads and Runways. *Géotechnique, Volume 1 Issue 4*, 249-263. Opgehaald van https://www.icevirtuallibrary.com/doi/abs/10.1680/geot.1949.1.4.249

Dong, Y.-L., Han, J., & Bai, X.-H. (2011). Numerical analysis of tensile behaviour of geogrids with rectangular and triangular apertures. *Geotextiles and Geomembranes*, 83-91. Retrieved from https://www.sciencedirect.com/science/article/abs/pii/S0266114410000890?via%3Dihub

EOTA. (2016). Non-reinforcing hexagonal geogrid for the stabilization of unbound granular layers by way of interlock with the aggregate. *Official Journal of the European Union*. Retrieved from https://www.eota.eu/en-GB/content/eads/56/

Huang, H., Tong, Q., Shushu, L., & Kwon, J. (2016). *Effect of Geogrid on Railroad Ballast Studied by "SmartRock".* The Pennsylvania State University, Pennsylvania. Retrieved March 23, 2019, from http://dx.doi.org/10.3141/2607-04

Jersey, S. R., & Tingle, J. S. (2010). *Full-Scale Accelerated Pavement Tests, Geogrid Reinforcement of Thin Asphalt Pavements, Phase 1 Interim Report.* US Army Corps of Engineers, Geotechnical and Structures Laboratory. Tensar International. Retrieved May 2, 2019

Kuljanski, L. (2016, March 14). Mechanistic-Empirical Pavement Analysis [PowerPoint slides]. Den Bosch.

Kuljanski, L. (2018). *O-25988 G183-011 Plot A te Bleiswijk.* Den Bosch: Tensar International. Retrieved May 12, 2019

Lay, M. G. (1993). *Ways of the world: a history of the world's roads and of the vehicles that used them.* Sydney: Primavera Press. Retrieved from https://trove.nla.gov.au/work/11494854?q&versionId=45429743

Lee, H. (2017). *Recommended Practise for Incorporating Geogrids in ME Pavement Design.* Champaign: Applied Research Associates. Retrieved from https://www.researchgate.net/publication/328571299_Recommended_Practice_for_Incorporating_Geogrids_in_ME_Pavement_Design

Marzurowski, P., Buckley, J., & Kawalec, J. (2019). *Modification of Mechanistic-Empirical pavement design method to incorporate the influence of hexagonal stabilisation geogrids.* Paper, Tensar, Sydney. Retrieved March 17, 2019

Modelling and Analysis Systems. (2005). *Rubicon Toolbox Training Course.* Modelling and Analysis Systems. Retrieved May 3, 2019, from www.modsys1.com

Norwood, G. J., & Tingle, J. J. (2014). *Performance of Geogrid-Stabilized Gravel Flexible Base with Bituminous Surface Treatment, Phase 2.* US Army Corps of Engineers, Engineer Research and Development Centre/Geotechnical and Structures Laboratory. US Army Engineer Research and Development Centre. Retrieved May 9, 2019, from http://acwc.sdp.sirsi.net/client/default

Tensar. (2012). Tensar Technology For use in the Oil and Gas Industry. Retrieved from https://www.tensar.co.uk/FileDownload.ashx?id=%7BB8BA9549-07A2-45C3-A967-D465A6D9FBF4%7D

Tensar. (2016). Spectra Pavement Optimisation System. Retrieved from www.tensarcorp.com/FileDownload.ashx?id=d2772f4b-24a0-4eea-8d26-e217147e332c

Tensar. (2017). *Selection of the appropriate Tensar TriAx Geogrid.*

Tensar. (2018). Tension membrane versus stabilisation [PowerPoint slides].

Tingle, J. S., Jeremy Robinson, W., & Norwood, G. J. (2017). *Full-Scale Accelerated Testing of Multi-axial Geogrid Stabilized Flexible Pavements, Phase 3.* US Army Corps of Engineers, Engineering Research and Development Centre/Geotechnical and Structures Laboratory. US Army Engineer Research and Development Centre. Retrieved May 18, 2019, from http://acwc.sdp.sirsi.net/client/en_US/default/

Tóth, E., Koren, C., Horvát, F., & Fischer, S. (2012). *Research Report of Laboratory Measurements of Geogrid-Reinforced Ballast Layer by Different Type of Tensar Geogrids in Multi-Level Shear Box in Respect to Railway Application.* Gyoer: UNIVERSITAT-GYÖR NONPROFIT Kft. Retrieved April 17, 2019, from www.univgyor.hu

van Gurp, C., de Bruijn, H., & van Putten, R. (2002). *Dunne asfaltverhardingen: dimensionering en herontwerp.* (R. de Groot, Ed.) Ede, The Netherlands: CROW media. Retrieved April 10, 2019, from www.crow.nl

van Gurp, C., van Vilsteren, I., van der Wegen, G., & Hofstra, U. (2014). *Handboek funderingsmaterialen in de wegenbouw.* Ede, The Netherlands: CROW media. Retrieved May 8, 2019, from www.crow.nl

Vega, E., Kwast, E., & van Gurp, C. (2017). *Geokunststoffen als funderingswapening in ongebonden funderingslagen.* Delft: SBRCURnet. Retrieved March 6, 2019

Yang, X. (2012). An assessment of the geometry effect of geosynthetics for base course reinforcement. *Transportation Science and Technology*, 247-257. Retrieved from https://www.sciencedirect.com/science/article/pii/S2046043016301617

You, Z., & Buttlar, W. (2004). Discrete Element Modeling to Predict the Modulus of Asphalt Concrete Mixtures. *Journal of Materials in Civil Engineering*. Retrieved from https://doi.org/10.1061/(ASCE)0899-1561(2004)16:2(140)

Zornberg, J. (2019). Functions and applications of geosynthetics in roadways. *Transportation Geotechnics and Geoecology* (pp. 298-306). Saint Petersburg: Elsevier Ltd. Retrieved from https://www.sciencedirect.com/science/article/pii/S1877705817321720

8 Appendix

Appendix A: SmartRock

Appendix B: GN and GH model

Appendix C: USACE phase 1 - 3 research results

Appendix D: ERApave - Calculation results sheet for USACE test sections

Appendix E: Screenshots of all USACE test sections in TensarPave

Appendix F: Project Waalwijk - Calculation information

Appendix G: Project Zuidplas - ERApave calculation result sheets

Appendix H: Large design variants drawing

Appendix I: Spectra Value Calculator reports

Appendix A

SmartRock

SmartRock Pennstate research results selection:

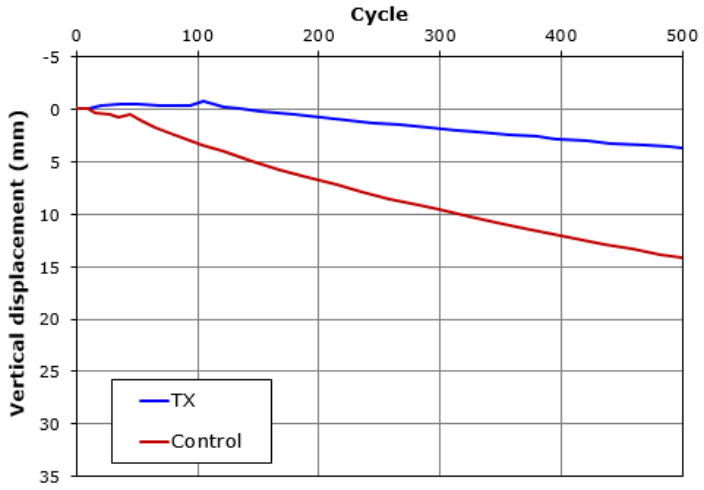

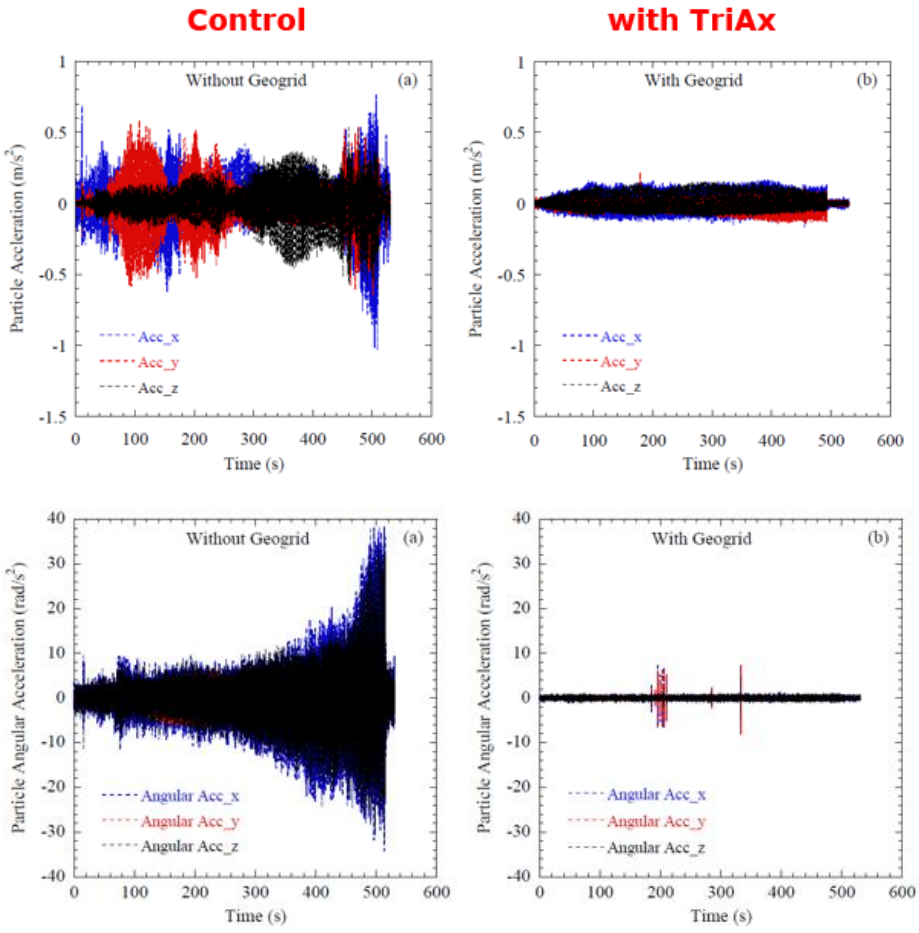

Appendix B

GN and GH model

The Giroud-Noiray and Giroud-Han models are two methods for calculating the thickness of a foundation layer and the thickness reduction due to inclusion of a geogrid or other type of reinforcement/stabilisation product. J.P. Giroud and L. Noiray published their paper “Geotextile-Reinforced unpaved road design” in 1981, proposing an empirical equation derived from full scale test on unpaved roads without reinforcement. A theoretical analysis is made to determine the foundation reduction factor from including a soil reinforcement product. In the third appendix of (Vega, Kwast, & van Gurp, 2017) an analysis of different design methods and their usability is made, including the GN and GH models.

The design method published by J.P. Giroud and J. Han in 2004 “The Giroud-Han design method for geosynthetic reinforced unpaved roads” continued the development of the GH-model from 1981. This new model offers the ability to determine the thickness of unreinforced and geogrid reinforced/stabilised foundation layers of unpaved roads on soils (subgrade) with low bearing capacity, while accounting for the change in stress distribution over time. The GN-model is the top picture and the GH-model is the bottom picture, retrieved from (Vega, Kwast, & van Gurp, 2017).

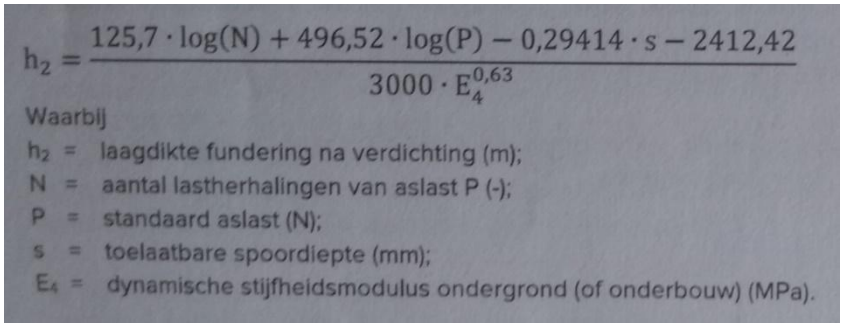

$$h_2 = \frac{125{,}7 \cdot \log(N) + 496{,}52 \cdot \log(P) - 0{,}29414 \cdot s - 2412{,}42}{3000 \cdot E_4^{0{,}63}}$$

Waarbij

h_2 = laagdikte fundering na verdichting (m);
N = aantal lastherhalingen van aslast P (-);
P = standaard aslast (N);
s = toelaatbare spoordiepte (mm);
E_4 = dynamische stijfheidsmodulus ondergrond (of onderbouw) (MPa).

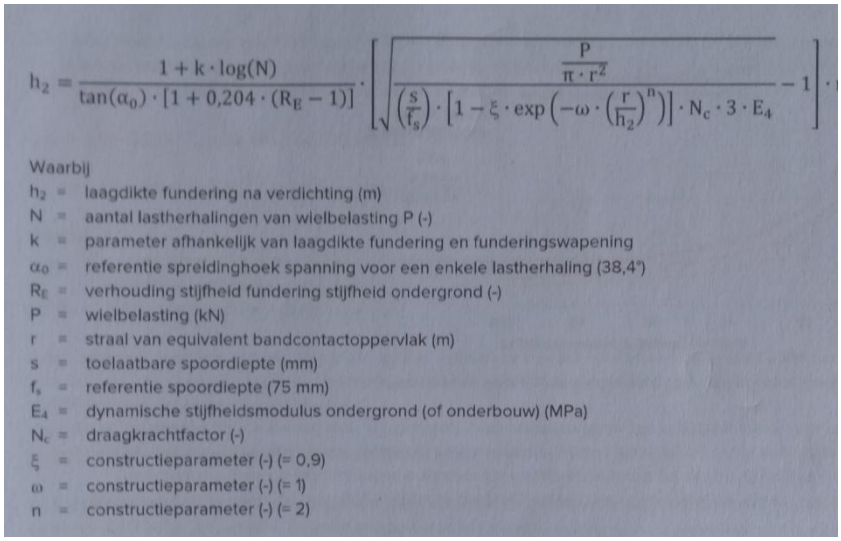

$$h_2 = \frac{1 + k \cdot \log(N)}{\tan(\alpha_0) \cdot [1 + 0{,}204 \cdot (R_E - 1)]} \cdot \left[\sqrt{\frac{\frac{P}{\pi \cdot r^2}}{\left(\frac{s}{f_s}\right) \cdot \left[1 - \xi \cdot \exp\left(-\omega \cdot \left(\frac{r}{h_2}\right)^n\right)\right] \cdot N_c \cdot 3 \cdot E_4}} - 1 \right] \cdot$$

Waarbij

h_2 = laagdikte fundering na verdichting (m)
N = aantal lastherhalingen van wielbelasting P (-)
k = parameter afhankelijk van laagdikte fundering en funderingswapening
α_0 = referentie spreidinghoek spanning voor een enkele lastherhaling (38,4°)
R_E = verhouding stijfheid fundering stijfheid ondergrond (-)
P = wielbelasting (kN)
r = straal van equivalent bandcontactoppervlak (m)
s = toelaatbare spoordiepte (mm)
f_s = referentie spoordiepte (75 mm)
E_4 = dynamische stijfheidsmodulus ondergrond (of onderbouw) (MPa)
N_c = draagkrachtfactor (-)
ξ = constructieparameter (-) (= 0,9)
ω = constructieparameter (-) (= 1)
n = constructieparameter (-) (= 2)

Appendix C

USACE phase 1 - 3 research results

USACE test sections			
Given name	From report	Item Nr.	Stabilised
1A	Phase 1	Item 1	Y
1B	Phase 1	Item 4	N
1C	Phase 1	Item 5	N
2A	Phase 2	Item 1	N
2B	Phase 2	Item 2	Y
3A	Phase 3	Item 1	Y
3B	Phase 3	Item 2	Y

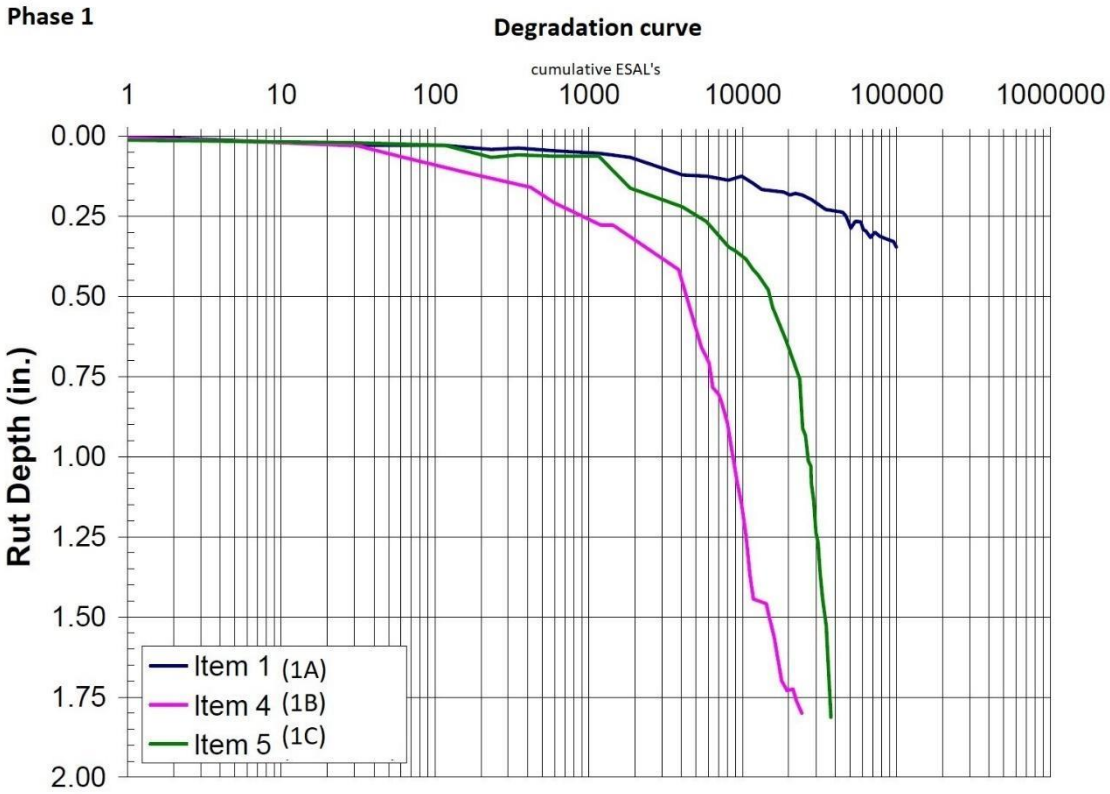

Phase 2

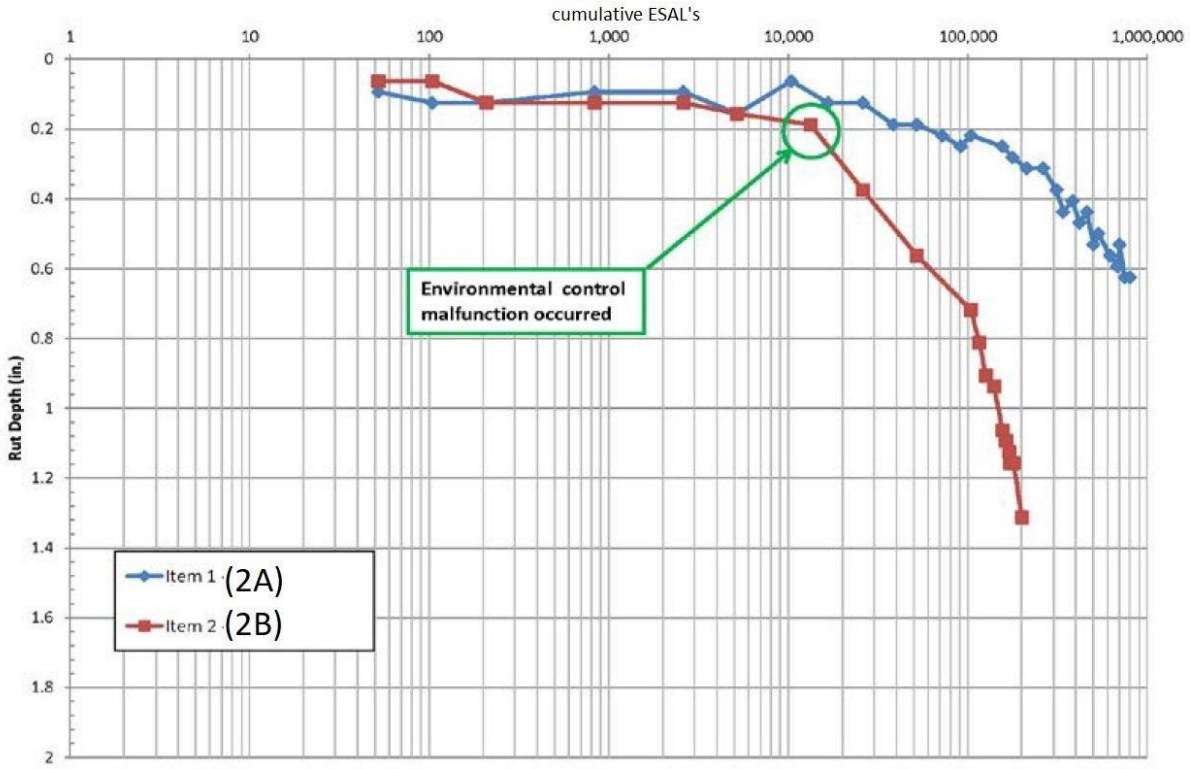

Phase 3

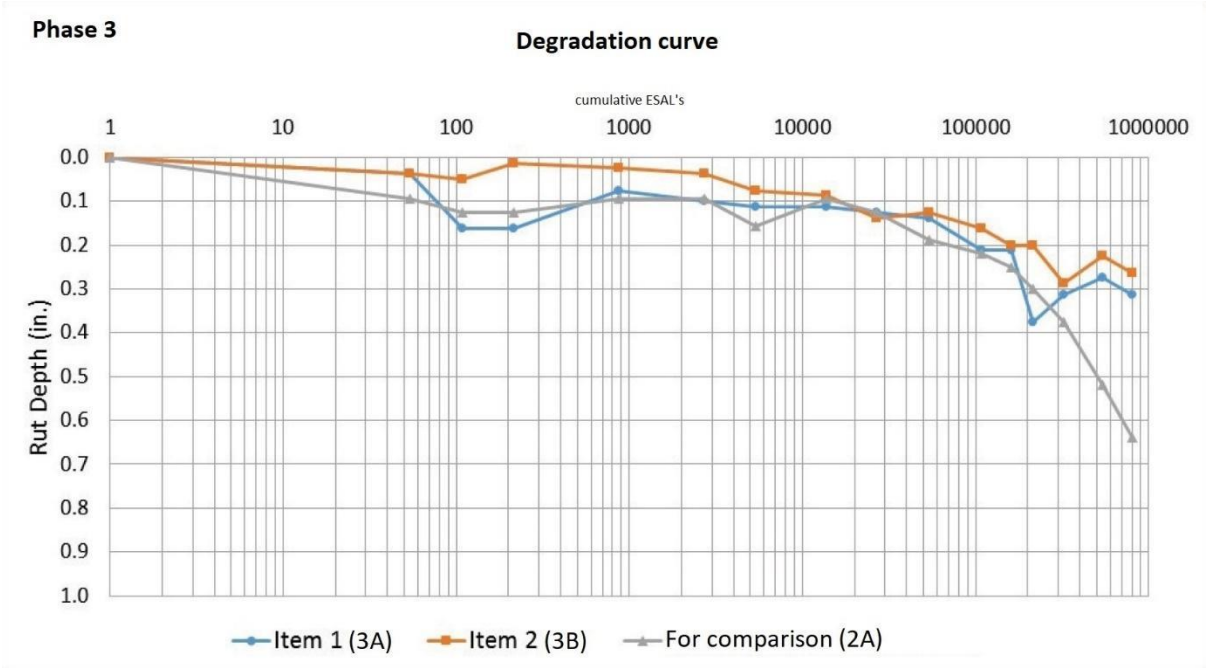

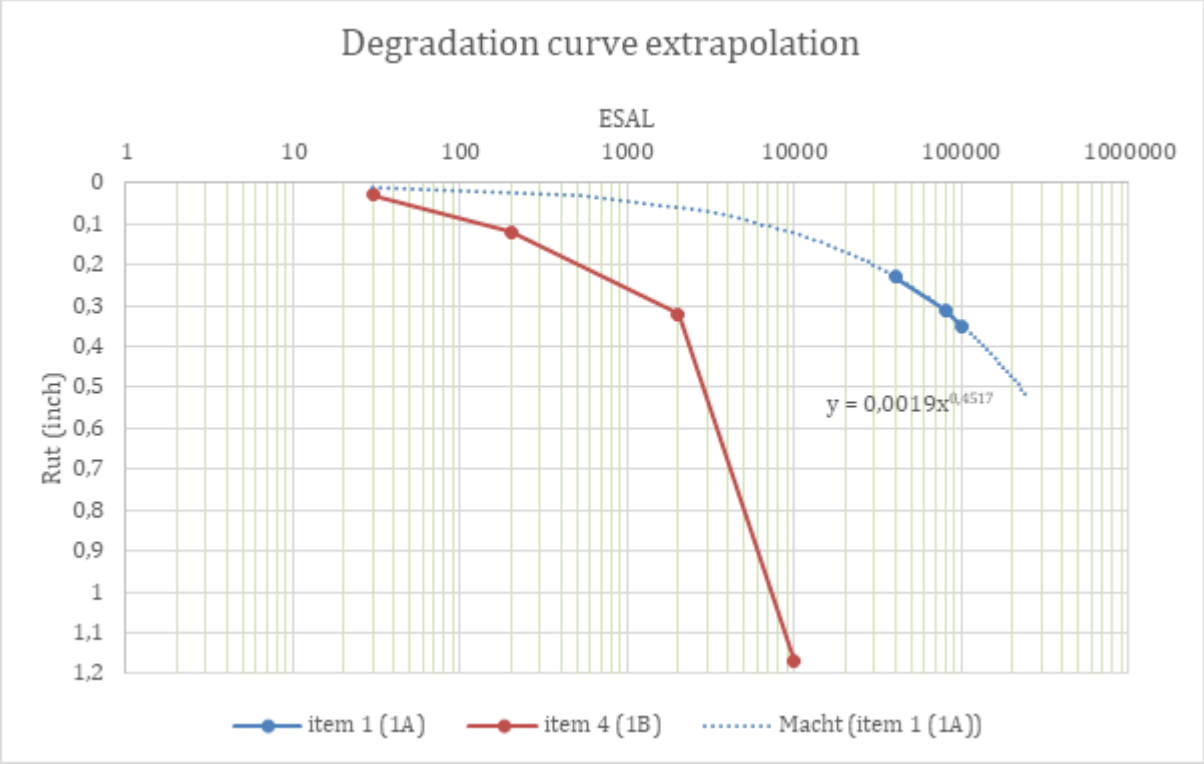
Degradation curve extrapolation
ESAL
1
10
100
1000
10000
100000
1000000
0
0,1
0,2
0,3
0,4
0,5
0,6
0,7
0,8
0,9
1
1,1
1,2
Rut (inch)
y = 0,0019x^0,4517
item 1 (1A)
item 4 (1B)
Macht (item 1 (1A))

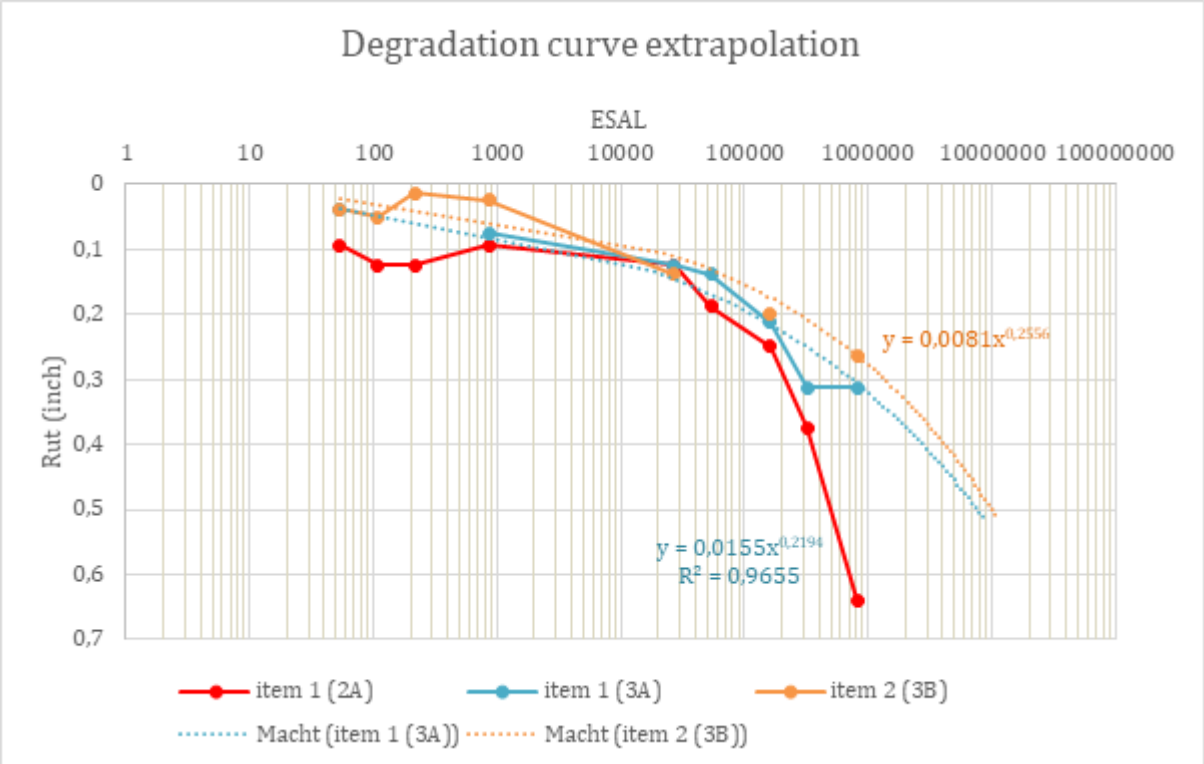
Degradation curve extrapolation
ESAL
1
10
100
1000
10000
100000
1000000
10000000
100000000
0
0,1
0,2
0,3
0,4
0,5
0,6
0,7
Rut (inch)
y = 0,0081x^0,2556
y = 0,0155x^0,2194
R² = 0,9655
item 1 (2A)
item 1 (3A)
item 2 (3B)
Macht (item 1 (3A))
Macht (item 2 (3B))

Phase 1

1A

50 mm asphalt
200mm aggregate base

1B

50 mm asphalt
200mm aggregate base

1C

75 mm asphalt
200mm aggregate base

Phase 2

2A

2B

ERROR IN TEST - NOT USED

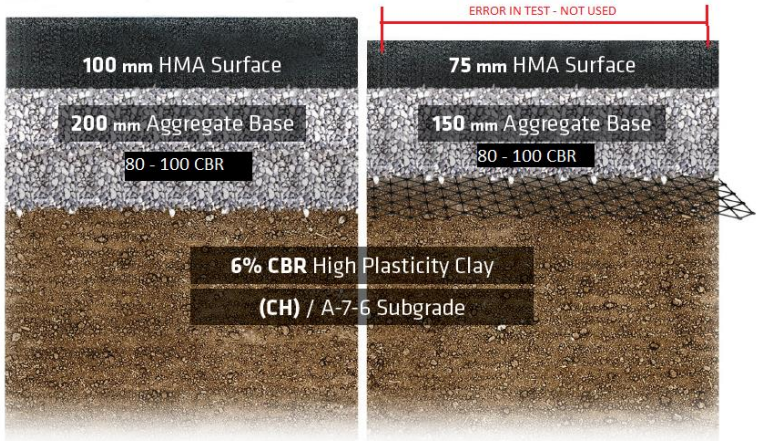

Phase 3

3A

3B

Only test sectionstabilised by TX8 geogrid

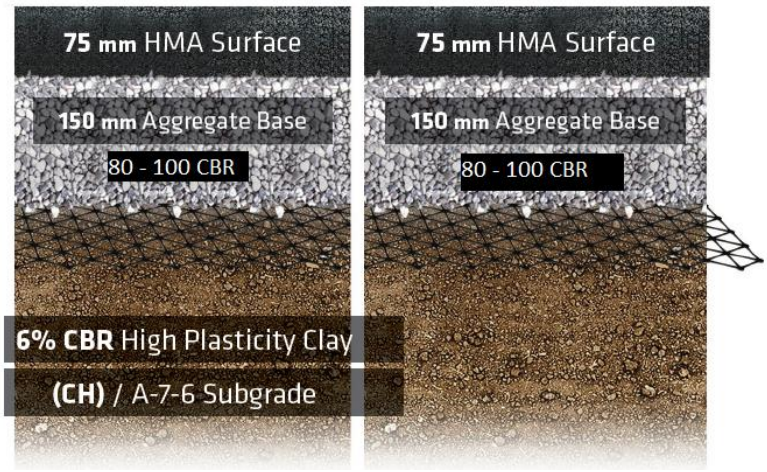

Appendix D

ERApave - calculation result sheets for USACE test sections

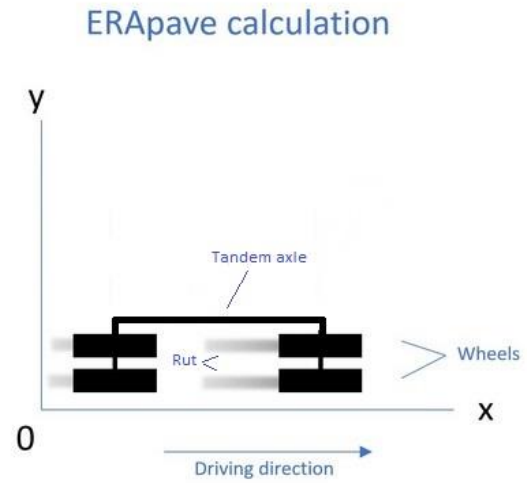

The ERApave results sheets from the USACE phase 1 - 3 test sections

SUMMARY OF INPUT DATA - PHASE 1 - ITEM 1 (1A)

MATERIAL PROPERTIES

Layer Id	Thickness [cm]	Modulus [MPa]	Poisson's ratio [-]	Unit weight [KN/m^3]
1	5.1	3054	0.35	23
2	20.3	700	0.35	14
3	1e+300	29.992	0.35	18

LOADING
Axle configuration :Tandem axle with dual wheels
Contact pressure [kPa] = 827
Axle load [kN] = 89
Wheel spacing [cm] = 35
Axle spacing [cm] = 117

STRESSES AND DISPLACEMENTS

x[cm]	y[cm]	z[cm]	szz[kPa]	sxx[kPa]	syy[kPa]	sxz[kPa]	syz[kPa]	sxy[kPa]	wz[cm]
0	0	5.09	451.415	-511.995	-488.061	-1.691	-19.193	-3.108	0.06992
0	17.5	5.09	19.244	83.749	366.124	-1.788	0	0	0.06756
58.5	17.5	5.09	1.668	50.426	99.329	0	0	0	0.06342
58.5	0	5.09	1.58	48.626	91.504	0	-5.964	0	0.06213

STRAINS

x[cm]	y[cm]	z[cm]	ezz[1e-3]	exx[1e-3]	eyy[1e-3]	exz[1e-3]	eyz[1e-3]	exy[1e-3]
0	0	5.09	0.262	-0.163	-0.153	-0.001	-0.017	-0.003
0	17.5	5.09	-0.045	-0.017	0.108	-0.002	0	0
58.5	17.5	5.09	-0.017	0.005	0.027	0	0	0
58.5	0	5.09	-0.016	0.005	0.024	0	-0.005	0

PRINCIPAL STRESSES

x[cm]	y[cm]	z[cm]	s1[kPa]	s2[kPa]	s3[kPa]
0	0	5.09	451.809	-488.041	-512.41
0	17.5	5.09	366.124	83.7986	19.1944
58.5	17.5	5.09	99.3293	50.4264	1.66792
58.5	0	5.09	91.8974	48.6256	1.18662

PRINCIPAL STRAINS

x[cm]	y[cm]	z[cm]	e1[1e-3]	e2[1e-3]	e3[1e-3]
0	0	5.09	0.263118	-0.152819	-0.164193
0	17.5	5.09	0.10808	-0.0166545	-0.0453433
58.5	17.5	5.09	0.0265541	0.00493692	-0.0166164
58.5	0	5.09	0.0248955	0.00525415	-0.0162293

EXCUTION TIME : 0.026Sec

SUMMARY OF INPUT DATA - PHASE 1 - ITEM 4 (1B)

MATERIAL PROPERTIES

Layer Id	Thickness [cm]	Modulus [MPa]	Poisson's ratio [-]	Unit weight [KN/m^3]
1	5.1	3054	0.35	23
2	20.3	212	0.35	14
3	1e+300	29.99	0.35	18

LOADING

Axle configuration :Single axle with dual wheels
Contact pressure [kPa] = 827
Axle load [kN] = 45
Wheel spacing [cm] = 35

STRESSES AND DISPLACEMENTS

x[cm]	y[cm]	z[cm]	szz[kPa]	sxx[kPa]	syy[kPa]	sxz[kPa]	syz[kPa]	sxy[kPa]	wz[cm]
0	0	5.09	287.745	-1635.3	-1551.08	0	-15.692	-0	0.07161
0	17.5	5.09	49.168	-271.519	459.506	0	0	0	0.06694
58.5	17.5	5.09	0.812	46.629	21.235	9.52	0	0	0.03407
58.5	0	5.09	0.77	43.399	21.099	8.686	-1.871	-4.302	0.03318
50	50	5.09	0.798	45.598	23.98	9.315	4.403	11.257	0.03424

STRAINS

x[cm]	y[cm]	z[cm]	ezz[1e-3]	exx[1e-3]	eyy[1e-3]	exz[1e-3]	eyz[1e-3]	exy[1e-3]
0	0	5.09	0.459	-0.391	-0.353	0	-0.014	-0
0	17.5	5.09	-0.005	-0.147	0.176	0	0	0
58.5	17.5	5.09	-0.008	0.013	0.002	0.008	0	0
58.5	0	5.09	-0.007	0.012	0.002	0.008	-0.002	-0.004
50	50	5.09	-0.008	0.012	0.003	0.008	0.004	0.01

PRINCIPAL STRESSES

x[cm]	y[cm]	z[cm]	s1[kPa]	s2[kPa]	s3[kPa]
0	0	5.09	287.879	-1551.21	-1635.3
0	17.5	5.09	459.506	49.1684	-271.519
58.5	17.5	5.09	48.5286	21.2349	-1.0873
58.5	0	5.09	45.9466	20.3004	-0.979203
50	50	5.09	52.4481	19.1898	-1.26145

PRINCIPAL STRAINS

x[cm]	y[cm]	z[cm]	e1[1e-3]	e2[1e-3]	e3[1e-3]
0	0	5.09	0.459627	-0.353687	-0.390678
0	17.5	5.09	0.175943	-0.00544438	-0.147202
58.5	17.5	5.09	0.0157826	0.00151618	-0.0105526
58.5	0	5.09	0.015676	0.000615422	-0.00988007
50	50	5.09	0.0211873	-0.00357582	-0.0106983

EXCUTION TIME : 0.028Sec

SUMMARY OF INPUT DATA - PHASE 1 - ITEM 5 (1C)

MATERIAL PROPERTIES

Layer Id	Thickness [cm]	Modulus [MPa]	Poisson's ratio [-]	Unit weight [KN/m^3]
1	7.6	3054	0.35	23
2	20.3	212	0.35	14
3	1e+300	28.958	0.35	18

LOADING

Axle configuration :Tandem axle with dual wheels
Contact pressure [kPa] = 827
Axle load [kN] = 89
Wheel spacing [cm] = 35
Axle spacing [cm] = 117

STRESSES AND DISPLACEMENTS

x[cm]	y[cm]	z[cm]	szz[kPa]	sxx[kPa]	syy[kPa]	sxz[kPa]	syz[kPa]	sxy[kPa]	wz[cm]
0	0	7.59	164.728	-1195.4	-1093.14	-1.015	-15.841	1.693	0.08096
0	17.5	7.59	55.51	-432.332	105.868	-1.073	0	0	0.08037
58.5	17.5	7.59	2.789	111.347	-15.775	0	0	0	0.06829
58.5	0	7.59	2.6	102.52	-9.063	0	-4.305	0	0.06662

STRAINS

x[cm]	y[cm]	z[cm]	ezz[1e-3]	exx[1e-3]	eyy[1e-3]	exz[1e-3]	eyz[1e-3]	exy[1e-3]
0	0	7.59	0.316	-0.285	-0.24	-0.001	-0.014	0.001
0	17.5	7.59	0.056	-0.16	0.078	-0.001	0	0
58.5	17.5	7.59	-0.01	0.038	-0.018	0	0	0
58.5	0	7.59	-0.01	0.034	-0.015	0	-0.004	0

PRINCIPAL STRESSES

x[cm]	y[cm]	z[cm]	s1[kPa]	s2[kPa]	s3[kPa]
0	0	7.59	164.928	-1093.31	-1195.43
0	17.5	7.59	105.868	55.5119	-432.335
58.5	17.5	7.59	111.347	2.78939	-15.7752
58.5	0	7.59	102.52	4.01636	-10.4802

PRINCIPAL STRAINS

x[cm]	y[cm]	z[cm]	e1[1e-3]	e2[1e-3]	e3[1e-3]
0	0	7.59	0.316567	-0.240122	-0.28507
0	17.5	7.59	0.0778505	0.0555943	-0.160061
58.5	17.5	7.59	0.0379477	-0.0100395	-0.0182459
58.5	0	7.59	0.0343098	-0.00784045	-0.0170336

EXCUTION TIME : 0.035Sec

SUMMARY OF INPUT DATA - PHASE 2 - ITEM 1 (2A)

MATERIAL PROPERTIES

Layer Id	Thickness [cm]	Modulus [MPa]	Poisson's ratio [-]	Unit weight [KN/m^3]
1	10.2	3054	0.35	23
2	20.3	206	0.35	14
3	1e+300	61.02	0.35	18

LOADING

Axle configuration :Tandem axle with dual wheels
Contact pressure [kPa] = 827
Axle load [kN] = 89
Wheel spacing [cm] = 35
Axle spacing [cm] = 117

STRESSES AND DISPLACEMENTS

x[cm]	y[cm]	z[cm]	szz[kPa]	sxx[kPa]	syy[kPa]	sxz[kPa]	syz[kPa]	sxy[kPa]	wz[cm]
0	0	10	110.237	-796.185	-706.677	-0.632	-11.827	1.602	0.04256
0	17.5	10	53.134	-389.262	-24.024	-0.666	0	0	0.04252
58.5	17.5	10	3.892	113.884	-15.839	0	0	0	0.03349
58.5	0	10	3.576	104.421	-9.21	0	-2.888	-0	0.03257

STRAINS

x[cm]	y[cm]	z[cm]	ezz[1e-3]	exx[1e-3]	eyy[1e-3]	exz[1e-3]	eyz[1e-3]	exy[1e-3]
0	0	10	0.208	-0.192	-0.153	-0.001	-0.01	0.001
0	17.5	10	0.065	-0.131	0.031	-0.001	0	0
58.5	17.5	10	-0.01	0.039	-0.019	0	0	0
58.5	0	10	-0.01	0.035	-0.015	0	-0.003	-0

PRINCIPAL STRESSES

x[cm]	y[cm]	z[cm]	s1[kPa]	s2[kPa]	s3[kPa]
0	0	10	110.409	-706.82	-796.214
0	17.5	10	53.135	-24.0237	-389.263
58.5	17.5	10	113.884	3.89176	-15.8395
58.5	0	10	104.421	4.19843	-9.83201

PRINCIPAL STRAINS

x[cm]	y[cm]	z[cm]	e1[1e-3]	e2[1e-3]	e3[1e-3]
0	0	10	0.208633	-0.153035	-0.192399
0	17.5	10	0.064764	0.0306553	-0.130798
58.5	17.5	10	0.0386594	-0.00996198	-0.018684
58.5	0	10	0.034837	-0.00875771	-0.0163753

EXCUTION TIME : 0.023Sec

Result sheet from phase 2 – item 2 (2B) is not included because an error occurred during the USACE test that made the data unreliable and thus unfit for use.

SUMMARY OF INPUT DATA - PHASE 3 - ITEM 1 (3A)

MATERIAL PROPERTIES

Layer Id	Thickness [cm]	Modulus [MPa]	Poisson's ratio [-]	Unit weight [KN/m^3]
1	8.1	3054	0.35	23
2	14.8	1400	0.35	14
3	1e+300	61.02	0.35	18

LOADING

Axle configuration :Tandem axle with dual wheels
Contact pressure [kPa] = 827
Axle load [kN] = 89
Wheel spacing [cm] = 35
Axle spacing [cm] = 117

STRESSES AND DISPLACEMENTS

x[cm]	y[cm]	z[cm]	szz[kPa]	sxx[kPa]	syy[kPa]	sxz[kPa]	syz[kPa]	sxy[kPa]	wz[cm]
0	0	8.09	331.826	-188.992	-173.651	-0.721	-21.569	-0.784	0.03699
0	17.5	8.09	23.62	-0.63	152.365	-0.79	0	0	0.03664
58.5	17.5	8.09	3.599	24.768	30.848	0	0	0	0.03346
58.5	0	8.09	3.411	23.527	28.775	0	-5.381	-0	0.03267

STRAINS

x[cm]	y[cm]	z[cm]	ezz[1e-3]	exx[1e-3]	eyy[1e-3]	exz[1e-3]	eyz[1e-3]	exy[1e-3]
0	0	8.09	0.15	-0.08	-0.073	-0.001	-0.019	-0.001
0	17.5	8.09	-0.01	-0.02	0.047	-0.001	0	0
58.5	17.5	8.09	-0.005	0.004	0.007	0	0	0
58.5	0	8.09	-0.005	0.004	0.006	0	-0.005	-0

PRINCIPAL STRESSES

x[cm]	y[cm]	z[cm]	s1[kPa]	s2[kPa]	s3[kPa]
0	0	8.09	332.745	-174.523	-189.039
0	17.5	8.09	152.365	23.646	-0.655507
58.5	17.5	8.09	30.8476	24.7678	3.5988
58.5	0	8.09	29.8688	23.5267	2.31696

PRINCIPAL STRAINS

x[cm]	y[cm]	z[cm]	e1[1e-3]	e2[1e-3]	e3[1e-3]
0	0	8.09	0.15183	-0.0747398	-0.0801175
0	17.5	8.09	0.0472554	-0.00960984	-0.0204201
58.5	17.5	8.09	0.0068498	0.00416227	-0.00519535
58.5	0	8.09	0.00808104	0.00401494	-0.00662325

EXCUTION TIME : 0.024Sec

SUMMARY OF INPUT DATA - PHASE 3 - ITEM 2 (3B)

MATERIAL PROPERTIES

Layer Id	Thickness [cm]	Modulus [MPa]	Poisson's ratio [-]	Unit weight [KN/m^3]
1	8.2	3054	0.35	23
2	15	1370	0.35	14
3	1e+300	61.02	0.35	18

LOADING

Axle configuration :Tandem axle with dual wheels
Contact pressure [kPa] = 827
Axle load [kN] = 89
Wheel spacing [cm] = 35
Axle spacing [cm] = 117

STRESSES AND DISPLACEMENTS

x[cm]	y[cm]	z[cm]	szz[kPa]	sxx[kPa]	syy[kPa]	sxz[kPa]	syz[kPa]	sxy[kPa]	wz[cm]
0	0	8.09	330.035	-184.283	-168.67	-0.763	-21.308	-0.804	0.03684
0	17.5	8.09	24.489	-0.553	152.383	-0.833	0	0	0.03647
58.5	17.5	8.09	3.562	24.96	31.313	0	0	0	0.03335
58.5	0	8.09	3.347	23.768	29.248	0	-5.374	-0	0.03257

STRAINS

x[cm]	y[cm]	z[cm]	ezz[1e-3]	exx[1e-3]	eyy[1e-3]	exz[1e-3]	eyz[1e-3]	exy[1e-3]
0	0	8.09	0.149	-0.079	-0.072	-0.001	-0.019	-0.001
0	17.5	8.09	-0.009	-0.02	0.047	-0.001	0	0
58.5	17.5	8.09	-0.005	0.004	0.007	0	0	0
58.5	0	8.09	-0.005	0.004	0.006	0	-0.005	-0

PRINCIPAL STRESSES

x[cm]	y[cm]	z[cm]	s1[kPa]	s2[kPa]	s3[kPa]
0	0	8.09	330.945	-169.531	-184.332
0	17.5	8.09	152.383	24.5169	-0.58081
58.5	17.5	8.09	31.3135	24.9601	3.56167
58.5	0	8.09	30.3187	23.7678	2.2762

PRINCIPAL STRAINS

x[cm]	y[cm]	z[cm]	e1[1e-3]	e2[1e-3]	e3[1e-3]
0	0	8.09	0.150116	-0.073423	-0.0789445
0	17.5	8.09	0.0471531	-0.00933279	-0.0205001
58.5	17.5	8.09	0.00698457	0.00417608	-0.00528293
58.5	0	8.09	0.00818431	0.00404703	-0.00669472

EXCUTION TIME : 0.033Sec

Appendix E

Screenshots of all USACE test sections in TensarPave

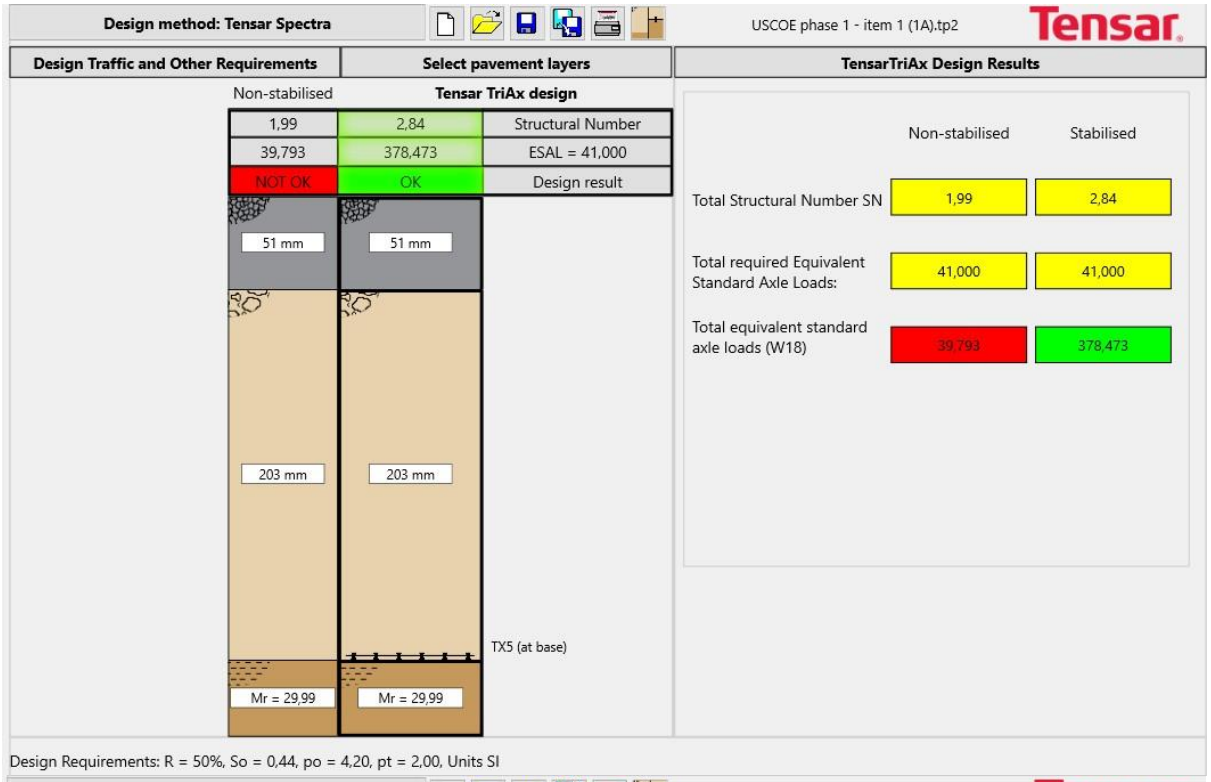
Design method: Tensar Spectra
USCOE phase 1 - item 1 (1A).tp2
Tensar
Design Traffic and Other Requirements
Select pavement layers
TensarTriAx Design Results
Non-stabilised
Tensar TriAx design
1,99
2,84
Structural Number
39,793
378,473
ESAL = 41,000
NOT OK
OK
Design result
51 mm
51 mm
203 mm
203 mm
TX5 (at base)
Mr = 29,99
Mr = 29,99
Non-stabilised
Stabilised
Total Structural Number SN
1,99
2,84
Total required Equivalent Standard Axle Loads:
41,000
41,000
Total equivalent standard axle loads (W18)
39,793
378,473
Design Requirements: R = 50%, So = 0,44, po = 4,20, pt = 2,00, Units SI

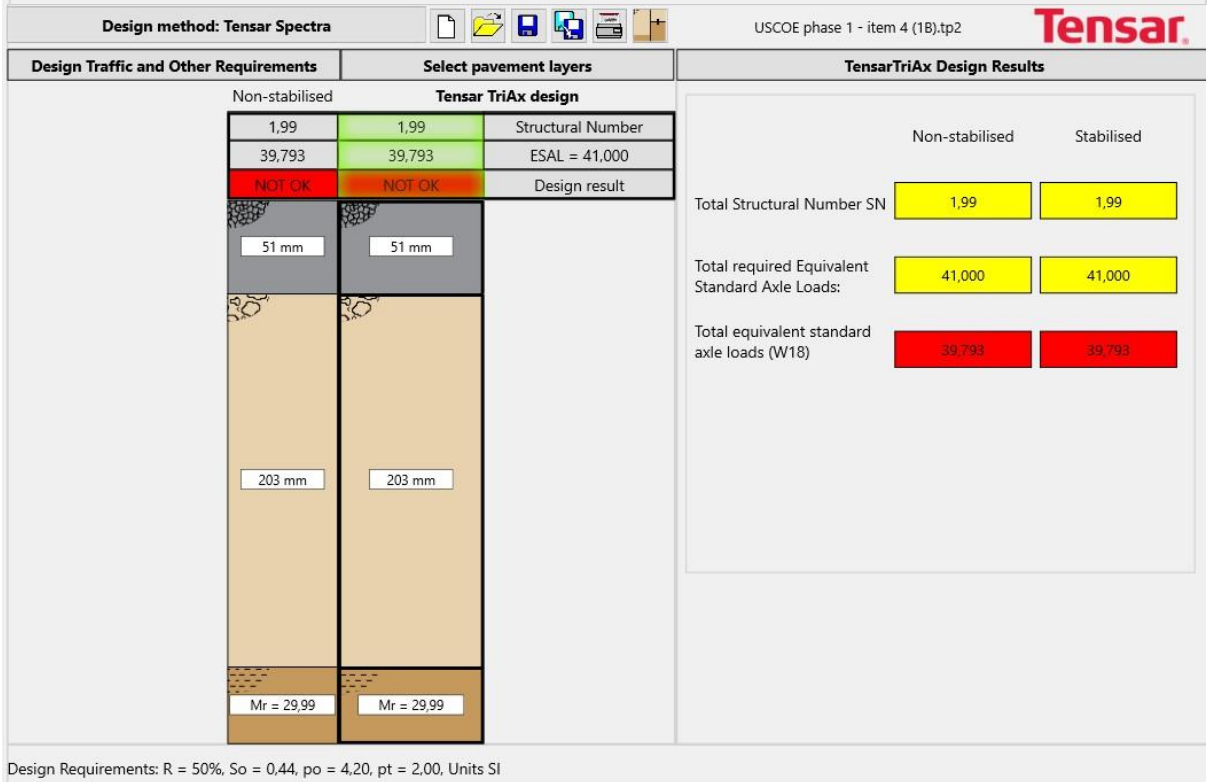
Design method: Tensar Spectra
USCOE phase 1 - item 4 (1B).tp2
Tensar
Design Traffic and Other Requirements
Select pavement layers
TensarTriAx Design Results
Non-stabilised
Tensar TriAx design
1,99
1,99
Structural Number
39,793
39,793
ESAL = 41,000
NOT OK
NOT OK
Design result
51 mm
51 mm
203 mm
203 mm
Mr = 29,99
Mr = 29,99
Non-stabilised
Stabilised
Total Structural Number SN
1,99
1,99
Total required Equivalent Standard Axle Loads:
41,000
41,000
Total equivalent standard axle loads (W18)
39,793
39,793
Design Requirements: R = 50%, So = 0,44, po = 4,20, pt = 2,00, Units SI

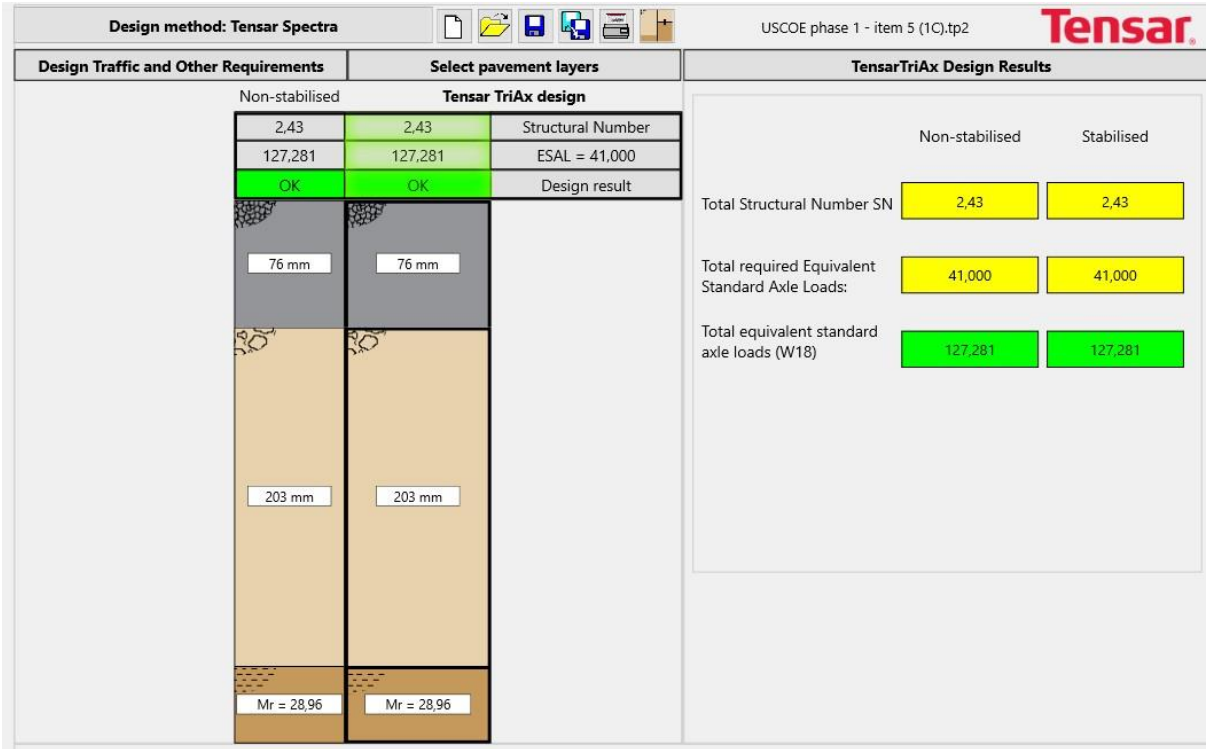

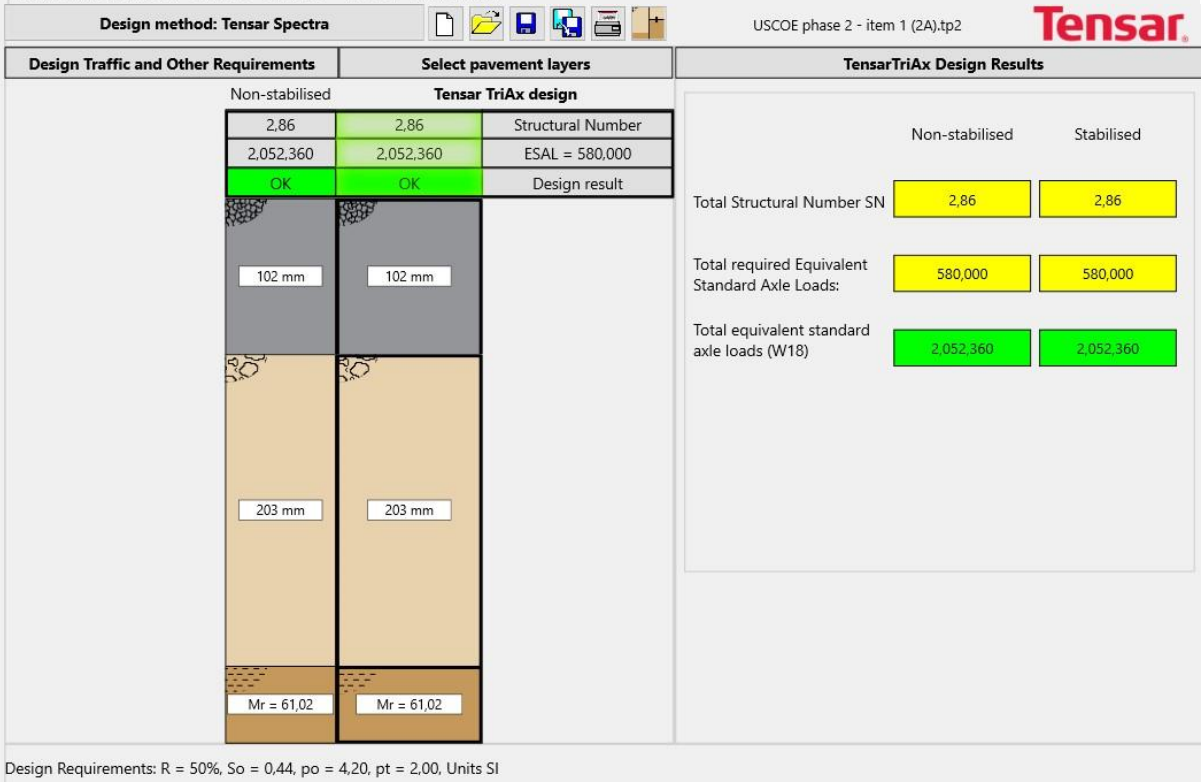

Phase 2 – item 2 (2B) is not included because an error occurred during the USACE test that made the data unreliable and thus unfit for use.

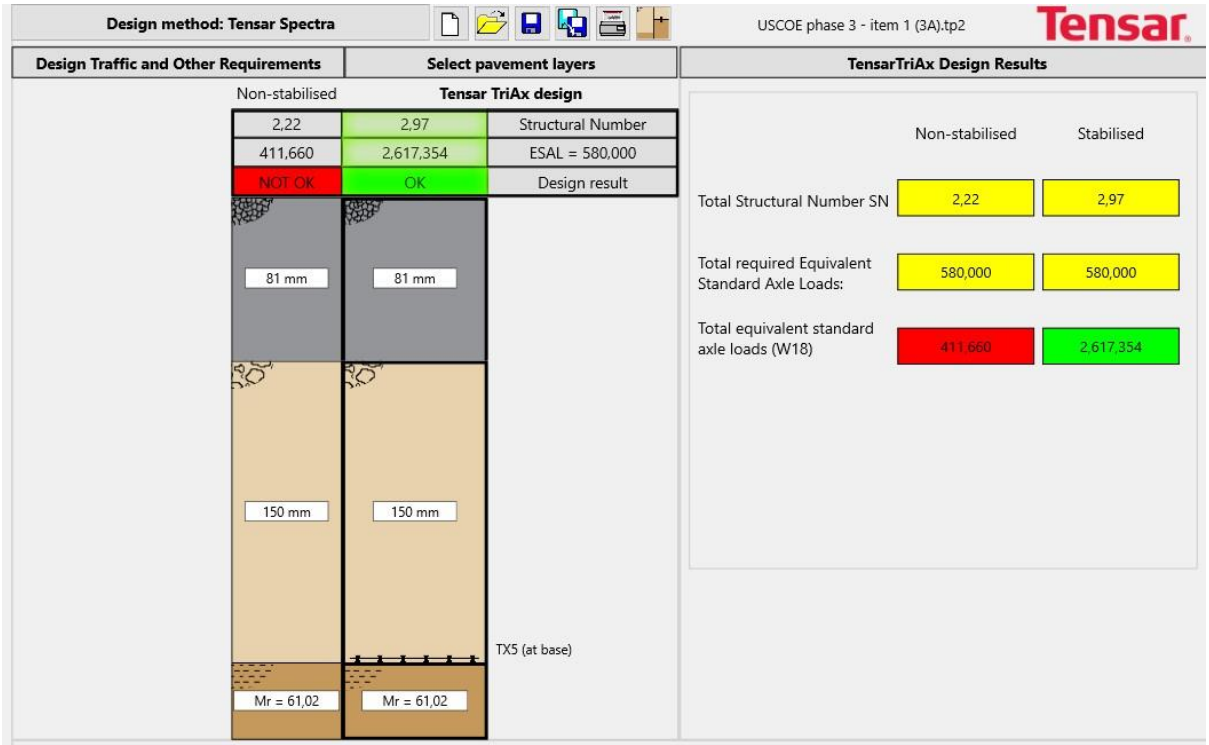
Design method: Tensar Spectra
USCOE phase 3 - item 1 (3A).tp2
Tensar
Design Traffic and Other Requirements
Select pavement layers
TensarTriAx Design Results
Non-stabilised
Tensar TriAx design
2,22
2,97
Structural Number
411,660
2,617,354
ESAL = 580,000
NOT OK
OK
Design result
81 mm
81 mm
150 mm
150 mm
TX5 (at base)
Mr = 61,02
Mr = 61,02
Non-stabilised
Stabilised
Total Structural Number SN
2,22
2,97
Total required Equivalent Standard Axle Loads:
580,000
580,000
Total equivalent standard axle loads (W18)
411,660
2,617,354
Design Requirements: R = 50%, So = 0,44, po = 4,20, pt = 2,00, Units SI

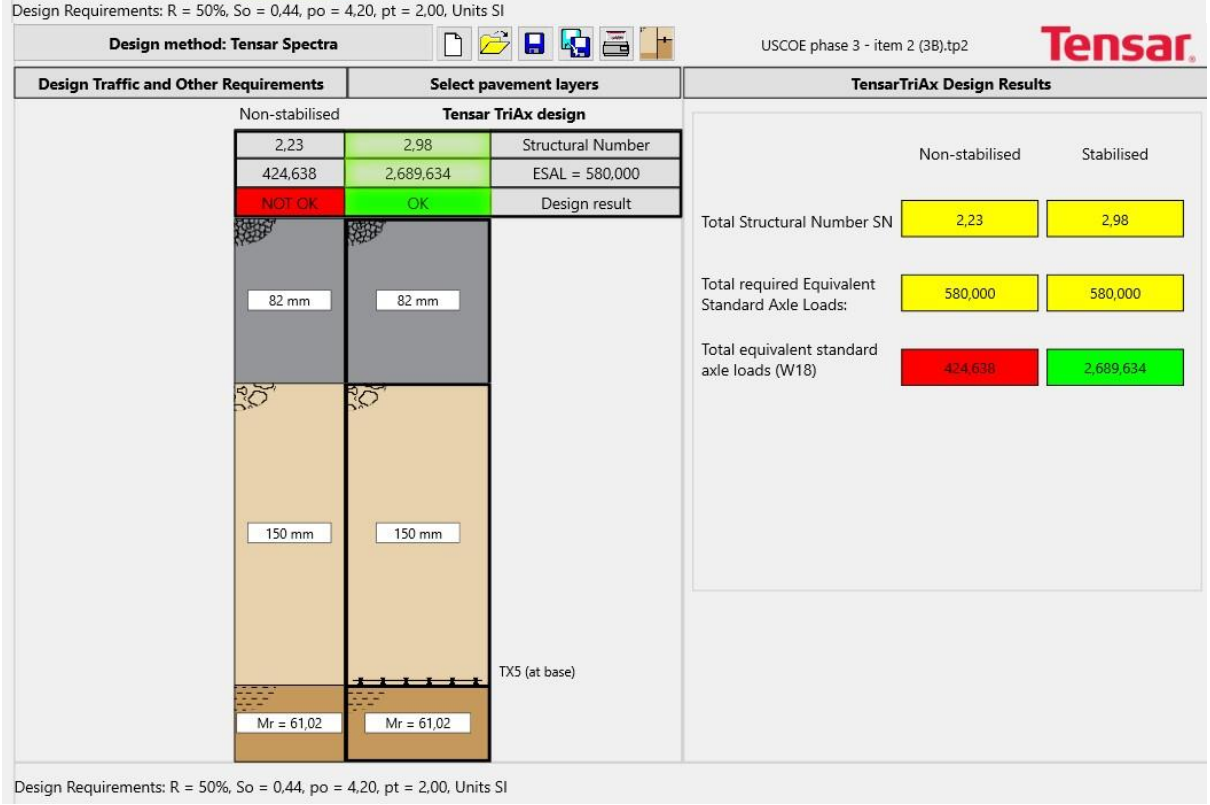
Design method: Tensar Spectra
USCOE phase 3 - item 2 (3B).tp2
Tensar
Design Traffic and Other Requirements
Select pavement layers
TensarTriAx Design Results
Non-stabilised
Tensar TriAx design
2,23
2,98
Structural Number
424,638
2,689,634
ESAL = 580,000
NOT OK
OK
Design result
82 mm
82 mm
150 mm
150 mm
TX5 (at base)
Mr = 61,02
Mr = 61,02
Non-stabilised
Stabilised
Total Structural Number SN
2,23
2,98
Total required Equivalent Standard Axle Loads:
580,000
580,000
Total equivalent standard axle loads (W18)
424,638
2,689,634
Design Requirements: R = 50%, So = 0,44, po = 4,20, pt = 2,00, Units SI

Appendix F

Project Waalwijk - calculation information

Retrieved from: 2019-006 RECON Waalwijk 300 MG.pdf

Ontwerpinstrumentarium Asfaltverhardingen

ATNL: Recon Grotestraat en Groen van Prinsterenlaan

Berekeningresultaat

Naam berekening	2019-006 RECON Waalwijk
Levensduur	Berekend 20 jaar.

Constructie

Laag	Naam	H mm	E MPa	Ss	Sf
Deklaag	SMA-NL 8B	25	3.000	1,000	1,000
TussenLaag	TL-IB 22	65	5.514	1,000	1,000
Onderlaag 1	RAW-onderlaagmengsel	81	6.726	1,000	1,000
Totaal		171	5.109		
Ongebonden fundering	Menggranulaat	300	400		
Ondergrond	Zand	-	100		

		Schade %	Criterium
Deklaag	SMA-NL 8B	0	Vermoeiing onderin
TussenLaag	TL-IB 22	0	Vermoeiing onderin
Onderlaag 1	RAW-onderlaagmengsel	100	Vermoeiing onderin
Ongebonden fundering	Menggranulaat		-
Ondergrond	Zand	3	Vervorming bovenop

Berekeningdetails

Constructielagen

Algemeen

Gefaseerd ontwerp	☐
Bereken dikte van de laag	**Onderlaag1**

Constructielagen

Deklaag	25 mm	[HUIDIG] SMA-NL 8B (S: -; ITSR: 80; B: 6,8)
TussenLaag	65 mm	[HUIDIG] TL-IB 22 (S: 5500; ε6: 80; fc: 0,2; ITSR: 70; HR: 6,5)
Onderlaag 1	81 mm	[HUIDIG] RAW-onderlaagmengsel (S: 8000; ε6: 105; fc: 0,2; ITSR: 70; HR: 4,5)
Totaal	171 mm	
Ongebonden fundering	300 mm	[HUIDIG] Menggranulaat (S: 400)
Ondergrond	- mm	[HUIDIG] Zand (S: 100)

Verkeer

Verkeersbelasting

Ontwerpperiode	**20,0** jaar	Aantal rijstroken per rijrichting	**1**
Aantal werkdagen per jaar	**270**	Rijstrookbreedte	**3,55** m
Snelheid vrachtverkeer	**50** km/u	Afst. kantstreep tot rand verhard.	**0,15** m

Aslastspectrum

Bereik	Rekenwaarde	%
20-40	30	8,67
40-60	50	40,71
60-80	70	25,97
80-100	90	13,66
100-120	110	8,05
120-140	130	2,18
140-160	150	0,38
160-180	170	0,38
180-220	190	0,00
200-220	210	0,00

Bandenspectrum

Band	%
DL	38,00
EL	39,00
BB	23,00
SB	0,00

Verkeersintensiteit

Herkomst verkeersbelasting	**Telling op nabij wegvak**	
	Fase 1	
Aantal motorvoertuigen per dag per richting	**300**	mvt/dag/ri
Percentage vrachtverkeer	**100**	%
Aantal vrachtauto's per dag per richting	**300**	vrw/dag/ri
Jaarlijkse groei	**1**	%

Drooglegging

Hoogteligging bovenzijde verharding t.o.v. NAP	**0,00** m
Hoogteligging grondwaterspiegel t.o.v. NAP	**0,00** m
Opbolling grondwaterspiegel	**0,00** m
Capilaire stijghoogte	**0,00** m
Restzetting	**0,00** m
Drooglegginsdiepte	**0,00** m
Vorstindringingsdiepte	**0,00** m

Ontwerpinstellingen

Betrouwbaarheid	75 %	Vermoeiing onder in asfalt	☑
Toelaatbaar schadepercentage	15 %	Verbrijzeling boven in fundering	☑
Ontwerpmode	**Standaard**	Breuk onder in gebonden fundering	☑
		Vermoeiing onder in gebonden fundering	☑
		Permanente deformatie in onder fundering	☑
		Permanente deformatie in ondergrond	☑

Tussenresultaat

Aslastklasse	Reken waarde	EL rek	DL rek	BB rek	SB rek
20-40	30	40	27	39	39
40-60	50	61	45	61	61
60-80	70	81	62	81	82
80-100	90	99	79	99	100
100-120	110	116	95	115	118
120-140	130	133	112	131	134
140-160	150	149	127	147	150
160-180	170	165	143	161	165
180-220	190	180	158	176	179
200-220	210	197	174	190	193

Toetsen

Asfalteigenschappen: Tussenlaag

- De watergevoeligheid is kleiner dan 80%.

Details van de constructielagen

Deklaag

Naam	**SMA-NL 8B**	Herkomst gegevens	
Type/Korrel/Toevoeging	**SMA - 8 B**	Toepasbaar als deklaag	☑
Minimum laagdikte	**15** mm	Toepasbaar als tussenlaag	☐
Maximum laagdikte	**30** mm	Toepasbaar als onderlaag	☐

Stijfheid

Poissongetal	**0,35**		
Karakteristieke frequentie	**0,0** Hz	C-getal	**0** °K
Stijfheidscoëfficiënt C1	**0,000000000**	Stijfheidscoëfficiënt C3	**0,000000000**
Stijfheidscoëfficiënt C2	**0,000000000**	Stijfheidscoëfficiënt C4	**0,000000000**

CE-gegevens

Bitumengehalte	**6,8** %	Holle ruimte	**0,0** %
ITSR	**80** %	Weerstand permanente vervorming	**0,0**
Stijfheidsmodulus (50%)	**0** MPa	Weerstand vermoeiing (50%)	**0** µm/m

Vermoeiing

Vermoeiingscoëfficiënt C1	**0**	Vermoeiingscoëfficiënt C4	**0**
Vermoeiingscoëfficiënt C2	**0**	Vermoeiingscoëfficiënt C5	**0**
Vermoeiingscoëfficiënt C3	**0**	Healingfactor	**0,00**

TussenLaag

Naam	**TL-IB 22**		Herkomst gegevens		
Type/Korrel/Toevoeging	**AC - 22**		Toepasbaar als deklaag	☐	
Minimum laagdikte	**50**	mm	Toepasbaar als tussenlaag	☑	
Maximum laagdikte	**90**	mm	Toepasbaar als onderlaag	☐	
Stijfheid					
Poissongetal	**0,35**				
Karakteristieke frequentie	**8,0**	Hz	C-getal	**11.242**	°K
Stijfheidscoëfficiënt C1	**9,419845151**		Stijfheidscoëfficiënt C3	**-0,001098345**	
Stijfheidscoëfficiënt C2	**-0,018400189**		Stijfheidscoëfficiënt C4	**0,000000000**	
CE-gegevens					
Bitumengehalte	**3,0**	%	Holle ruimte	**6,5**	%
ITSR	**70**	%	Weerstand permanente vervorming	**0,2**	
Stijfheidsmodulus (50%)	**5.500**	MPa	Weerstand vermoeiing (50%)	**80**	µm/m
Vermoeiing					
Vermoeiingscoëfficiënt C1	**39,176619630 0687**		Vermoeiingscoëfficiënt C4	**-0,6953733627 23148**	
Vermoeiingscoëfficiënt C2	**-0,0644494450 589267**		Vermoeiingscoëfficiënt C5	**-0,2126107343 96086**	
Vermoeiingscoëfficiënt C3	**1,4043632480 2624**		Healingfactor	**4,00**	

Onderlaag 1

Naam	**RAW-onderlaagmengsel**		Herkomst gegevens		
Type/Korrel/Toevoeging	**AC - 16**		Toepasbaar als deklaag	☐	
Minimum laagdikte	**25**	mm	Toepasbaar als tussenlaag	☐	
Maximum laagdikte	**60**	mm	Toepasbaar als onderlaag	☑	
Stijfheid					
Poissongetal	**0,35**				
Karakteristieke frequentie	**8,0**	Hz	C-getal	**11.242**	°K
Stijfheidscoëfficiënt C1	**9,618546968**		Stijfheidscoëfficiënt C3	**-0,001098345**	
Stijfheidscoëfficiënt C2	**-0,018400189**		Stijfheidscoëfficiënt C4	**0,000000000**	
CE-gegevens					
Bitumengehalte	**3,0**	%	Holle ruimte	**4,5**	%
ITSR	**70**	%	Weerstand permanente vervorming	**0,2**	
Stijfheidsmodulus (50%)	**8.000**	MPa	Weerstand vermoeiing (50%)	**105**	µm/m
Vermoeiing					
Vermoeiingscoëfficiënt C1	**39,176585**		Vermoeiingscoëfficiënt C4	**-1,058189**	
Vermoeiingscoëfficiënt C2	**-0,064449**		Vermoeiingscoëfficiënt C5	**-0,212611**	
Vermoeiingscoëfficiënt C3	**1,404363**		Healingfactor	**4,00**	

Ongebonden fundering

Naam	**Menggranulaat**		Herkomst gegevens		
Stijfheidsmodulus	**400**	MPa	Poissongetal	**0,35**	
Toelaatbare buigtrekspanning	**128**	KPa	Zelfbindende fundering	☐	

Ondergrond

Naam	**Zand**		Herkomst gegevens		
Stijfheidsmodulus	**100**	MPa	Poissongetal	**0,35**	

Appendix G

Project Zuidplas - ERApave calculation result sheets

SUMMARY OF INPUT DATA - STANDARD UNSTABILISED DESIGN

MATERIAL PROPERTIES

Layer Id	Thickness [cm]	Modulus [MPa]	Poisson's ratio [-]	Unit weight [KN/m^3]
1	4	2300	0.35	23
2	4	2800	0.35	23
3	13.5	3400	0.35	23
4	30	200	0.35	14
5	100	50	0.35	14
6	1e+300	20	0.35	18

LOADING

Axle configuration :Single axle with dual wheels
Contact pressure [kPa] = 800
Axle load [kN] = 70
Wheel spacing [cm] = 50

STRESSES AND DISPLACEMENTS

x[cm]	y[cm]	z[cm]	szz[kPa]	sxx[kPa]	syy[kPa]	sxz[kPa]	syz[kPa]	sxy[kPa]	wz[cm]
0	0	21.49	43.336	-476.868	-409.085	0	-6.964	-0	0.05012
0	25	21.49	28.262	-330.402	-139.583	0	0	0	0.05075
58.5	25	21.49	5.924	9.451	-66.163	9.999	0	0	0.04117
58.5	0	21.49	5.461	8.31	-57.896	9.195	-2.757	-21.978	0.04034

STRAINS

x[cm]	y[cm]	z[cm]	ezz[1e-3]	exx[1e-3]	eyy[1e-3]	exz[1e-3]	eyz[1e-3]	exy[1e-3]
0	0	21.49	0.104	-0.103	-0.076	0	-0.006	-0
0	25	21.49	0.057	-0.086	-0.01	0	0	0
58.5	25	21.49	0.008	0.009	-0.021	0.008	0	0
58.5	0	21.49	0.007	0.008	-0.018	0.007	-0.002	-0.017

PRINCIPAL STRESSES

x[cm]	y[cm]	z[cm]	s1[kPa]	s2[kPa]	s3[kPa]
0	0	21.49	43.4436	-409.192	-476.868
0	25	21.49	28.2618	-139.583	-330.402
58.5	25	21.49	17.8407	-2.46566	-66.1627
58.5	0	21.49	20.9076	-0.504157	-64.5276

PRINCIPAL STRAINS

x[cm]	y[cm]	z[cm]	e1[1e-3]	e2[1e-3]	e3[1e-3]
0	0	21.49	0.104117	-0.075861	-0.102605
0	25	21.49	0.0566931	-0.00995109	-0.0857176
58.5	25	21.49	0.0162516	0.000309437	-0.0210423
58.5	0	21.49	0.0206151	0.00269446	-0.0272029

EXCUTION TIME : 0.047Sec

SUMMARY OF INPUT DATA - MAXIMUM STABILISED VARIANT

MATERIAL PROPERTIES

Layer Id	Thickness [cm]	Modulus [MPa]	Poisson's ratio [-]	Unit weight [KN/m^3]
1	4	2300	0.35	23
2	4	2800	0.35	23
3	13.5	3400	0.35	23
4	30	660	0.35	14
5	100	50	0.35	14
6	1e+300	20	0.35	18

LOADING

Axle configuration :Single axle with dual wheels
Contact pressure [kPa] = 800
Axle load [kN] = 70
Wheel spacing [cm] = 50

STRESSES AND DISPLACEMENTS

x[cm]	y[cm]	z[cm]	szz[kPa]	sxx[kPa]	syy[kPa]	sxz[kPa]	syz[kPa]	sxy[kPa]	wz[cm]
0	0	21.49	77.976	-258.876	-223.725	0	-11.906	-0	0.04228
0	25	21.49	33.394	-149.193	-17.479	0	0	0	0.04248
58.5	25	21.49	2.888	11.742	-22.965	16.337	0	0	0.03645
58.5	0	21.49	2.75	10.788	-20.499	15.042	-4.398	-9.301	0.0359

STRAINS

x[cm]	y[cm]	z[cm]	ezz[1e-3]	exx[1e-3]	eyy[1e-3]	exz[1e-3]	eyz[1e-3]	exy[1e-3]
0	0	21.49	0.073	-0.061	-0.047	0	-0.009	-0
0	25	21.49	0.027	-0.046	0.007	0	0	0
58.5	25	21.49	0.002	0.006	-0.008	0.013	0	0
58.5	0	21.49	0.002	0.005	-0.007	0.012	-0.003	-0.007

PRINCIPAL STRESSES

x[cm]	y[cm]	z[cm]	s1[kPa]	s2[kPa]	s3[kPa]
0	0	21.49	78.445	-224.194	-258.876
0	25	21.49	33.3942	-17.4793	-149.193
58.5	25	21.49	24.2415	-9.61131	-22.9654
58.5	0	21.49	24.588	-8.49061	-23.0583

PRINCIPAL STRAINS

x[cm]	y[cm]	z[cm]	e1[1e-3]	e2[1e-3]	e3[1e-3]
0	0	21.49	0.0733553	-0.047921	-0.0611366
0	25	21.49	0.0269793	0.00677952	-0.0455187
58.5	25	21.49	0.0168548	-0.00826058	-0.0093297
58.5	0	21.49	0.017911	-0.00704502	-0.0114802

EXCUTION TIME : 0.036Sec

SUMMARY OF INPUT DATA - OPTIMISED STABILISED VARIANT

MATERIAL PROPERTIES

Layer Id	Thickness [cm]	Modulus [MPa]	Poisson's ratio [-]	Unit weight [KN/m^3]
1	4	2300	0.35	23
2	2.5	2800	0.35	23
3	9	3400	0.35	23
4	30	660	0.35	14
5	50	50	0.35	14
6	1e+300	20	0.35	18

LOADING

Axle configuration :Single axle with dual wheels
Contact pressure [kPa] = 800
Axle load [kN] = 70
Wheel spacing [cm] = 50

STRESSES AND DISPLACEMENTS

x[cm]	y[cm]	z[cm]	szz[kPa]	sxx[kPa]	syy[kPa]	sxz[kPa]	syz[kPa]	sxy[kPa]	wz[cm]
0	0	15.49	139.572	-366.777	-332.163	0	-13.787	-0	0.05231
0	25	15.49	36.431	-117.286	75.894	0	0	0	0.05208
58.5	25	15.49	1.417	29.357	0.62	18.428	0	0	0.04351
58.5	0	15.49	1.42	27.944	0.863	16.98	-4.894	-6.631	0.04278

STRAINS

x[cm]	y[cm]	z[cm]	ezz[1e-3]	exx[1e-3]	eyy[1e-3]	exz[1e-3]	eyz[1e-3]	exy[1e-3]
0	0	15.49	0.113	-0.088	-0.074	0	-0.011	-0
0	25	15.49	0.015	-0.046	0.031	0	0	0
58.5	25	15.49	-0.003	0.008	-0.003	0.015	0	0
58.5	0	15.49	-0.003	0.008	-0.003	0.013	-0.004	-0.005

PRINCIPAL STRESSES

x[cm]	y[cm]	z[cm]	s1[kPa]	s2[kPa]	s3[kPa]
0	0	15.49	139.975	-332.565	-366.777
0	25	15.49	75.8942	36.4305	-117.286
58.5	25	15.49	38.5114	0.619773	-7.73804
58.5	0	15.49	37.9985	-0.569343	-7.20255

PRINCIPAL STRAINS

x[cm]	y[cm]	z[cm]	e1[1e-3]	e2[1e-3]	e3[1e-3]
0	0	15.49	0.113638	-0.0749441	-0.0880499
0	25	15.49	0.0306452	0.0149758	-0.0460588
58.5	25	15.49	0.0185277	-0.00298556	-0.0127722
58.5	0	15.49	0.0191457	-0.00471356	-0.0117651

EXCUTION TIME : 0.034Sec

SUMMARY OF INPUT DATA - SAME COST STABILISED VARIANT

MATERIAL PROPERTIES

Layer Id	Thickness [cm]	Modulus [MPa]	Poisson's ratio [-]	Unit weight [KN/m^3]
1	4	2300	0.35	23
2	4	2800	0.35	23
3	12.5	3400	0.35	23
4	30	660	0.35	14
5	100	50	0.35	14
6	1e+300	20	0.35	18

LOADING

Axle configuration :Single axle with dual wheels
Contact pressure [kPa] = 800
Axle load [kN] = 70
Wheel spacing [cm] = 50

STRESSES AND DISPLACEMENTS

x[cm]	y[cm]	z[cm]	szz[kPa]	sxx[kPa]	syy[kPa]	sxz[kPa]	syz[kPa]	sxy[kPa]	wz[cm]
0	0	20.49	85.325	-272.688	-237.075	0	-12.209	-0	0.04311
0	25	20.49	34.211	-146.548	-5.557	0	0	0	0.04326
58.5	25	20.49	2.716	14.911	-19.515	16.633	0	0	0.03691
58.5	0	20.49	2.591	13.859	-17.338	15.311	-4.451	-9.069	0.03635

STRAINS

x[cm]	y[cm]	z[cm]	ezz[1e-3]	exx[1e-3]	eyy[1e-3]	exz[1e-3]	eyz[1e-3]	exy[1e-3]
0	0	20.49	0.078	-0.065	-0.05	0	-0.01	-0
0	25	20.49	0.026	-0.046	0.01	0	0	0
58.5	25	20.49	0.001	0.006	-0.008	0.013	0	0
58.5	0	20.49	0.001	0.006	-0.007	0.012	-0.004	-0.007

PRINCIPAL STRESSES

x[cm]	y[cm]	z[cm]	s1[kPa]	s2[kPa]	s3[kPa]
0	0	20.49	85.7866	-237.537	-272.688
0	25	20.49	34.2114	-5.55661	-146.548
58.5	25	20.49	26.5289	-8.90283	-19.5147
58.5	0	20.49	26.8021	-7.90104	-19.7895

PRINCIPAL STRAINS

x[cm]	y[cm]	z[cm]	e1[1e-3]	e2[1e-3]	e3[1e-3]
0	0	20.49	0.0783013	-0.0511706	-0.0645811
0	25	20.49	0.02572	0.00992975	-0.0460521
58.5	25	20.49	0.0171227	-0.00755406	-0.00973527
58.5	0	20.49	0.0181684	-0.00731403	-0.0109327

EXCUTION TIME : 0.036Sec

Appendix H

Large design variants drawing

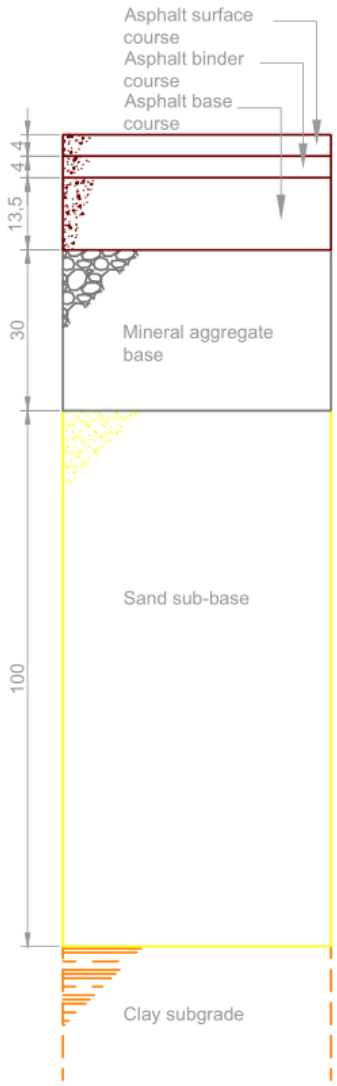

Variant 1:
unstabilised (standard)
4.307.581 ESAL
20 y. design life*

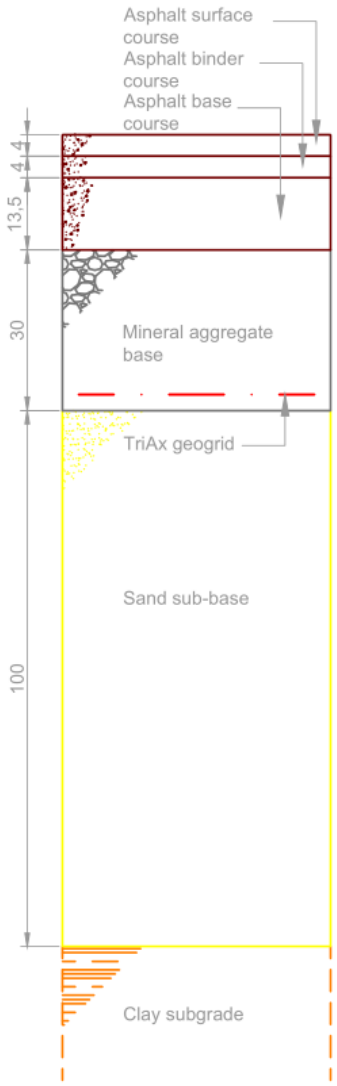

Variant 2:
stabilised (maximum)
35.800.883 ESAL
90 y. design life

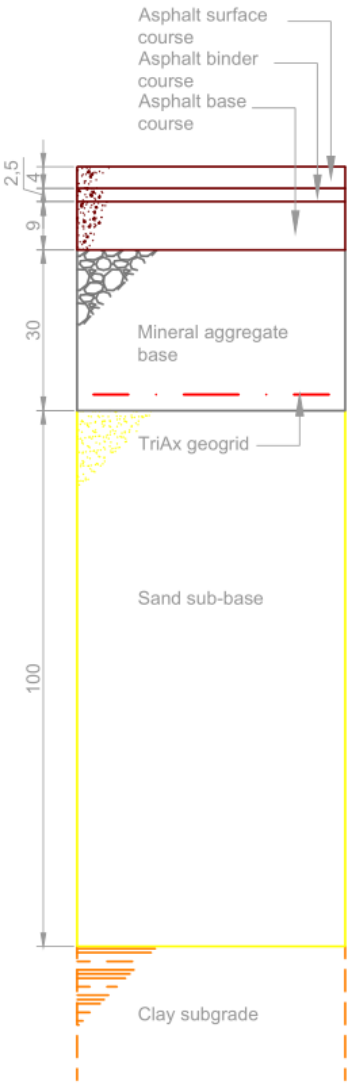

Variant 3:
stabilised (optimised)
4.857.180 ESAL
21 y. design life

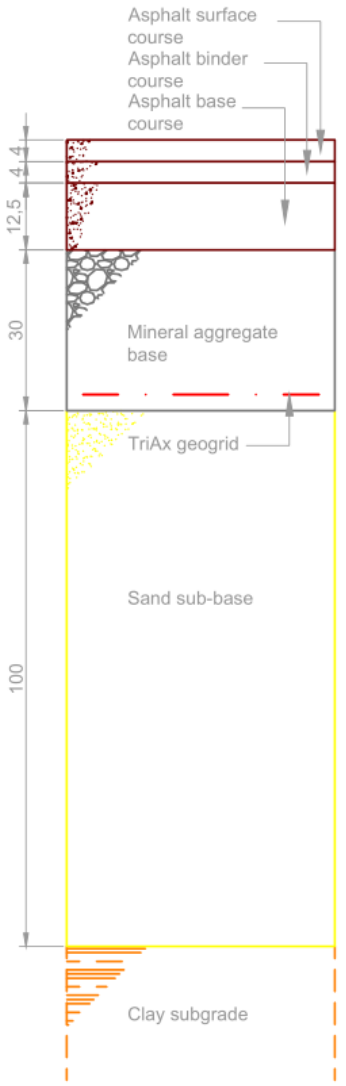

Variant 4:
stabilised (same cost)
27.408.149 ESAL
77 y. design life

Appendix I

Spectra Value Calculator reports

Tensar | THE COMPANY YOU CAN BUILD ON™

Spectra Value Calculator

Output Report

stabilised (maximum)

Client	
Project Name	zuidplas
Project Reference	unst. + st. Max
Document Reference	
Date	10/07/2019

Geosynthetics Used	Non-stabilised	Tensar MSL
Position 3	-	Y
Position 2	-	N
Position 1	N	N

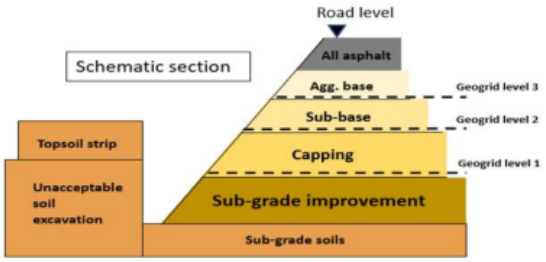

CONSTRUCTION COST BENEFIT

	Non-stabilised		Tensar MSL		Estimated Saving	
Construction Cost	-	*less*	-	=	-	EUR
Volume of Aggregate	-	*less*	-	=	-	m^3
Mass of Aggregate	-	*less*	-	=	-	t
Truck Deliveries *(All Layers)*	-	*less*	-	=	-	trucks

TIME BENEFIT

	Non-stabilised		Tensar MSL		Estimated Saving	
Project Critical Path Time	-	*less*	-	=	-	days
Total Activity Time	-	*less*	-	=	-	days

LIFE CYCLE COST BENEFIT

	Non-stabilised	Tensar MSL	Estimated Saving
Initial Construction	-	-	-
Maintenance	-	-	-
Rehabilitation	-	-	-
Salvage	-	-	-

Total Life Cycle Cost	-	*less*	-	=	-	EUR

CARBON FOOTPRINT

	Non-stabilised		Tensar MSL		Estimated Saving	
Carbon Usage ($kgCO_2e$)	828.972	*less*	833.283	=	(4.310)	$kgCO_2e$

Tensar International Ltd

T: +44(0)1254 262431
F: +44(0)1254 266868

Units 2-4 Cunningham Court
Shadsworth Business Park
Blackburn, UK
BB1 2QX

Version: Germany v6.05

Tensar | THE COMPANY YOU CAN BUILD ON™

Spectra Value Calculator

Output Report

stabilised (optimised)

Client	
Project Name	zuidplas
Project Reference	unst. + st. Opt.
Document Reference	
Date	10/07/2019

Geosynthetics Used	Non-stabilised	Tensar MSL
Position 3	-	Y
Position 2	-	N
Position 1	N	N

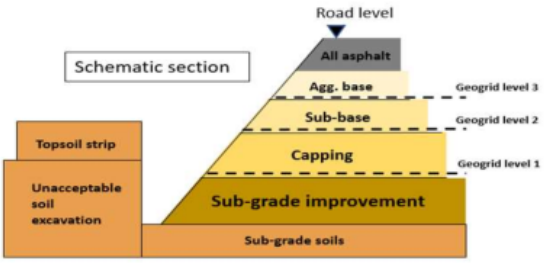

CONSTRUCTION COST BENEFIT

	Non-stabilised		Tensar MSL		Estimated Saving	
Construction Cost	-	*less*	-	=	-	EUR
Volume of Aggregate	-	*less*	-	=	-	m^3
Mass of Aggregate	-	*less*	-	=	-	t
Truck Deliveries *(All Layers)*	-	*less*	-	=	-	trucks

TIME BENEFIT

	Non-stabilised		Tensar MSL		Estimated Saving	
Project Critical Path Time	-	*less*	-	=	-	days
Total Activity Time	-	*less*	-	=	-	days

LIFE CYCLE COST BENEFIT

	Non-stabilised		Tensar MSL		Estimated Saving	
Initial Construction	-		-		-	
Maintenance	-		-		-	
Rehabilitation	-		-		-	
Salvage	-		-		-	
Total Life Cycle Cost	-	*less*	-	=	-	EUR

CARBON FOOTPRINT

	Non-stabilised		Tensar MSL		Estimated Saving	
Carbon Usage ($kgCO_2e$)	828.972	*less*	769.299	=	59.673	$kgCO_2e$

Tensar International Ltd

T: +44(0)1254 262431
F: +44(0)1254 266868

Units 2-4 Cunningham Court
Shadsworth Business Park
Blackburn, UK
BB1 2QX

Version: Germany v6.05

Tensar | THE COMPANY YOU CAN BUILD ON™

Spectra Value Calculator

Output Report

stabilised (same cost)

Client	
Project Name	zuidplas
Project Reference	unst. + st. S. Cost
Document Reference	
Date	10/07/2019

Geosynthetics Used	Non-stabilised	Tensar MSL
Position 3	-	Y
Position 2	-	N
Position 1	N	N

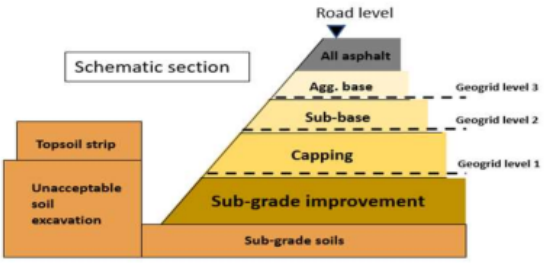

CONSTRUCTION COST BENEFIT

	Non-stabilised		Tensar MSL		Estimated Saving	
Construction Cost	-	*less*	-	=	-	EUR
Volume of Aggregate	-	*less*	-	=	-	m^3
Mass of Aggregate	-	*less*	-	=	-	t
Truck Deliveries *(All Layers)*	-	*less*	-	=	-	trucks

TIME BENEFIT

	Non-stabilised		Tensar MSL		Estimated Saving	
Project Critical Path Time	-	*less*	-	=	-	days
Total Activity Time	-	*less*	-	=	-	days

LIFE CYCLE COST BENEFIT

	Non-stabilised		Tensar MSL		Estimated Saving	
Initial Construction	-		-		-	
Maintenance	-		-		-	
Rehabilitation	-		-		-	
Salvage	-		-		-	
Total Life Cycle Cost	-	*less*	-	=	-	EUR

CARBON FOOTPRINT

	Non-stabilised		Tensar MSL		Estimated Saving	
Carbon Usage ($kgCO_2e$)	828.972	*less*	822.589	=	6.384	$kgCO_2e$

Tensar International Ltd

T: +44(0)1254 262431
F: +44(0)1254 266868

Units 2-4 Cunningham Court
Shadsworth Business Park
Blackburn, UK
BB1 2QX

Version: Germany v6.05